UNIVERSITA' DEGLI STUDI DI VERONA

DEPARTMENT OF

MEDICINE

GRADUATE SCHOOL OF

MEDICINE AND SURGERY

DOCTORAL PROGRAM IN

BIOMOLECULAR MEDICINE

Cycle / year (1° year of attendance): XXXIII

TITLE OF THE DOCTORAL THESIS

ONC212 IS A NOVEL MITOCAN ACTING SYNERGISTICALLY WITH GLYCOLYSIS INHIBITION IN PANCREATIC CANCER

S.S.D. MED/06

Coordinator: Prof. Massimo Donadelli

Signature _____

Tutor: Prof. Carlo Visco

Signature _____

Doctoral Student: Dott. Isacco Ferrarini

Signature _____

SOMMARIO

L'adenocarcinoma del pancreas è al quattordicesimo posto tra le neoplasie maligne più comuni e la settima causa di morte per cancro nel mondo. Si tratta di una neoplasia spesso diagnosticata in fase avanzata e frequentemente poco responsiva ai trattamenti disponibili, peraltro gravati da una significativa tossicità. Per questi motivi, è necessario trovare nuovi composti attivi in questa neoplasia.

Gli imipridoni costituiscono una classe di molecole ad azione antineoplastica di recente scoperta. Il capostipite ONC201 si è dimostrato efficace in diversi modelli pre-clinici di neoplasie solide ed ematologiche, ed è tuttora testato in studi clinici di fase I/II per neoplasie recidivate/refrattarie. Gli imipridoni presentano un effetto anti-proliferativo e talvolta pro-apoptotico mediato dall'attivazione della risposta integrata allo stress e dall'induzione trascrizionale di recettori di morte cellulare, in particolare DR5. Più recentemente, è stato scoperto che ONC201 e il suo più potente derivato fluorinato ONC212 devono parte del loro effetto antineoplastico all'interazione con ClpP, una peptidasi mitocondriale coinvolta nella fisiologica degradazione di proteine mitocondriali danneggiate. In particolare, ONC201 e ONC212 alterano la normale conformazione di ClpP e inducono uno stato di iperattività enzimatica tale per cui vengono degradate in maniera incontrollata proteine coinvolte in vari aspetti del metabolismo mitocondriale.

In questo studio, abbiamo valutato l'effetto di ONC212 in modelli pre-clinici di carcinoma del pancreas. I risultati ottenuti mostrano che ClpP, considerato il target di ONC212, è ampiamente espressa in cellule umane di carcinoma del pancreas ed è necessaria per l'azione anti-proliferativa di ONC212. Nonostante ONC212 riduca la produzione di ATP di origine mitocondriale e blocchi la crescita in tutte le linee cellulari, soltanto in alcune di esse viene inibita la via delle MAPK (considerata una delle principali vie di sopravvivenza in questa neoplasia a causa delle frequenti mutazioni di Ras) e viene innescata l'apoptosi. Studi metabolici funzionali hanno mostrato come le linee cellulari in grado di resistere all'apoptosi indotta da ONC212 aumentassero il flusso glicolitico. In queste cellule, l'assenza di glucosio nel terreno di coltura o il trattamento concomitante con l'inibitore della glicolisi 2-desossiglucosio (2-DG) risultava

sinergico con ONC212, e favoriva l'inibizione della via delle MAPK e la conseguente apoptosi. In modelli murini trapiantati con una linea cellulare umana di carcinoma pancreatico resistente a ONC212, la combinazione di ONC212 e 2-DG risultava efficace nel rallentare la crescita tumorale e priva di significativa tossicità. L'analisi immunoistochimica delle masse tumorali ha mostrato inoltre che la terapia di combinazione, ma non gli agenti singoli, determinava riduzione della proliferazione e induzione di apoptosi, valutati tramite i marcatori Ki67 e caspasi 3 clivata, rispettivamente.

Nel complesso, ONC212 può essere considerato un nuovo agente mitocondriotossico sinergico con inibitori della via glicolitica e con potenzialità di sviluppo clinico nel carcinoma del pancreas.

ABSTRACT

ONC212 is a fluorinated-imipridone with preclinical efficacy against pancreatic and other malignancies. Although mitochondrial protease ClpP was identified as an ONC212-binding target, the mechanism leading to cancer cell death is incompletely understood. We investigated mitochondrial dysfunction and metabolic rewiring triggered by ONC212 in pancreatic cancer, a deadly malignancy with an urgent need for novel therapeutics. We found ClpP is expressed in pancreatic cancer cells and is required for ONC212 cytotoxicity. ClpX, the regulatory binding-partner of ClpP, is suppressed upon ONC212 treatment. Immunoblotting and extracellular flux analysis showed ONC212 impairs oxidative phosphorylation (OXPHOS) with decrease in mitochondrial-derived ATP production. Although collapse of mitochondrial function is observed across ONC212-treated cell lines, only OXPHOS-dependent cells undergo apoptosis. Cells relying on glycolysis undergo growth-arrest and upregulate glucose catabolism to prevent ERK1/2 inhibition and apoptosis. Glucose restriction or combination with glycolytic inhibitor 2-deoxy-D-glucose synergize with ONC212 and promote apoptosis *in vitro* and *in vivo*. Thus, ONC212 is a novel mitocan targeting oxidative-metabolism in pancreatic cancer, leading to different cellular outcomes based on divergent metabolic programs.

INDEX

1. INTRODUCTION

1.1 Pancreatic adenocarcinoma

Pancreatic adenocarcinoma (PDAC) is the most common type of pancreatic tumor. PDAC incidence is rising; it is expected to become the second cause of cancer-related death by 2030 and carries a very poor prognosis. More than 80% of patients have an advanced disease at diagnosis, and the 5-year overall survival rate is about 7%. Poor survival is attributed to high aggressiveness, intrinsic resistance to chemotherapeutics, and lack of effectively targetable oncogenic drivers. Systemic chemotherapy is the mainstay of locally advanced and metastatic patients treatment and gemcitabine monotherapy had been the standard for more than two decades until first-line FOLFIRINOX and nab-paclitaxel/gemcitabine demonstrated better efficacy. Targeted therapies have a limited role in PDAC management. Therefore, new therapeutic approaches with meaningful impact on patient survival are urgently needed (1).

Recently, substantial progress was made in the understanding of PDAC genetic background and molecular biology. Up to 4 molecular subtypes have been identified, each with distinct molecular signatures potentially targetable with specific drugs. These valuable research efforts, however, have not yet been matched either by the successful development of novel agents or by the identification of predictive biomarkers that could increase the efficacy of existing therapies. As a result, PDAC remains refractory to most currently available treatments. Moreover, the peculiar tumor microenvironment with the excessive desmoplastic stroma represents an important biological barrier for drug delivery and activity. In this regard, however, targeting components of the tumor stroma that contribute to desmoplasia emerged as a potential therapeutic approach (1). Several genomic and epigenomic studies revealed significant molecular heterogeneity among PDAC. Recently, Bailey et al. suggested the existence of 4 molecular subtypes with different biological features and prognostic relevance: squamous, pancreatic progenitor, immunogenic and aberrantly differentiated endocrine exocrine (ADEX). This classification was based on the differential

expression of crucial transcription factors and downstream targets in lineage differentiation during pancreatic development (2).

From a metabolic viewpoint, pancreatic cancer utilizes both oxidative phosphorylation (OXPHOS) and aerobic glycolysis to produce bioenergy. OXPHOS is an energy extracting process in which pyruvate enters the mitochondria matrix via pyruvate translocase and is oxidized to generate ATP, H_2O, and CO_2. Oxygen acts as a final electron acceptor in the electron transport chain. As a result of the associated redox reactions, an electrochemical potential originates across the inner mitochondrial membrane, which drives a proton-motive force across the membrane, and directly results in ATP biosynthesis. Thus, carbon flows through the tricarboxylic acid (TCA) cycle and is oxidized to its simplest form, creating energy subunits with high energy phosphate bonds that guide other chemical reactions required for cell viability. Well-perfused and differentiated normal cells produce the bulk of their cellular energy through OXPHOS in the mitochondria. Cancer cells, on the other hand, are often oxygen-poor. This scenario theoretically hinders effective OXPHOS. Even in the presence of sufficient oxygen, however, scientists believed for decades that cancer cells were metabolically reprogrammed (3).

Scientists posited that cancer cells relied on cytosolic glycolysis to produce ATP instead of OXPHOS, even though the energy yield was far less efficient (2 ATP vs. 36 ATP). A bias towards aerobic glycolysis is eponymously referred to as the “Warburg's effect”, and there have been numerous evidences that in fact reveal robust glycolytic activity in pancreatic cancer cells in several experimental models, including patient samples. For instance, endogenous expression of many glycolytic enzymes is increased, including hexokinase 2, enolase 2, and lactate dehydrogenases. As a consequence, glycolytic metabolites, including lactate, are also elevated in pancreatic cancer cells. Generally speaking, a biochemical penchant for glycolysis can favor tumor growth in multiple ways. First, lactic acid build-up reduces cellular and extracellular pH. This contributes to invasiveness by promoting genetic changes in PDAC cells, impairing the anti-tumor immune response (protecting cancer cells from immune patrol), reducing adherens junctions on cancer cell membranes (facilitating detachment and metastases), and

hydrolysis of extracellular proteins to facilitate cell invasion. Furthermore, enhanced glycolytic activity minimizes combustion of carbon from glucose to CO_2. Instead, organic carbon is preserved, and diverted into cellular building blocks through biosynthetic pathways, such as lipid synthesis, the hexosamine biosynthesis pathway, and the pentose phosphate pathway (3). This reprogramming effort promotes the macromolecular synthesis, which is needed for cell proliferation (i.e., anabolism). As stated above for desmoplasia, oncogenic KRAS drives glycolytic activity in PDAC. For example, KRAS activation leads to increased glucose uptake and elevated levels of glycolysis-associated metabolites (3).

Despite these data, the classic Warburg model misses an important part of the story. Current perspectives maintain that a balance between aerobic glycolysis and OXPHOS is much more complex, and seems to be highly variable among different tumor types. Moreover, the balance is not fixed in a given tumor. Rather, the metabolic program is dynamic, and responds to microenvironment conditions. Contrary to Warburg's teachings, mitochondria in cancer are often fully functional, and aerobic respiration is even critical for cancer cell survival. A preponderance of new evidence shows that pancreatic cancer cells are dependent on mitochondrial OXPHOS under low nutrient conditions, and that mitochondrial metabolism represents a key metabolic vulnerability (3).

An siRNA screen of 2,752 metabolic genes revealed that mitochondrial genes encoding electron transport chain proteins were functionally the most important genes in cancer cell survival under low glucose conditions. In addition, when 28 cell lines were evaluated for their ability to withstand low glucose conditions, resistant cell lines consistently augmented oxygen consumption on demand, as compared to the most vulnerable cell lines (4). Further, the vulnerable cell lines exhibited higher rates of genetic mutations in mitochondria-encoded electron transport genes. All of these findings suggest that cancer cells adapting to harsh and unfavorable metabolic conditions prioritize the conservation of glucose, and rewire their biology to maximize energy yields through enhanced mitochondrial respiration. Such metabolic shift ensures the production of sufficient ATP to fuel critical cellular processes. Under austere conditions, cancer cells choose to divert

carbon away from biosynthetic pathways, which minimizes unnecessary ATP consumption. Cell proliferation is deferred for a later time when energy supplies become more available, or cancer cells become more adept at scavenging nutrients from a deprived microenvironment (3).

Therefore, it stands to reason that mitochondrial biology represents a promising therapeutic target in PDAC. There are some clinical studies that support this idea in pancreatic cancer patients. For example, a common anti-diabetic drug, metformin, inhibits complex 1 of the electron transport chain. A meta-analysis of nine retrospective studies and two randomized clinical studies in PDAC patients revealed that metformin assumption was associated with prolonged survival (5).

1.2 The mitochondrial peptidase ClpP

Caseinolytic peptidase P (ClpP) proteolytic complex is a multimeric serine protease expressed in many prokaryotes and the mitochondria of eukaryotic cells and chloroplasts. This peptidase complex has been comprehensively studied in bacteria, whereas its role in mammalian cells is less understood (6).

Mitochondria are intracellular double membrane organelles that convert energy-carrying molecules into ATP through the process of OXPHOS. In addition to energy production, mitochondria regulate several other critical cellular functions such as reactive oxygen species (ROS) generation, calcium homeostasis, macromolecule biogenesis (i.e., protein and nucleic acids), lipid synthesis, intrinsic apoptosis, and antioxidant protection. Mitochondria contain their own genetic heritage, termed mitochondrial DNA (mtDNA) which is ~16.7 kb and encodes 13 mitochondrial proteins constituting essential subunits within the respiratory chain. With the exception of respiratory chain complex II, all respiratory chain complexes have protein subunits that are encoded by mitochondrial DNA (6). While mitochondria encode for 13 proteins, the remaining 99% of mitochondrial proteins are encoded by nuclear genes, which are translated in the cytosol and imported into the mitochondria *via* targeting sequences. The abundance of mitochondrial proteins depends on the transcription, mRNA processing, translation efficiency, protein stability, and degree of mitochondrial targeting. Mitochondria possess multiple mechanisms to preserve

optimal protein structure and function, including the proper folding of newly imported proteins and the degradation of damaged or misfolded ones. Maintaining mitochondrial protein homeostasis is mediated by a panel of specialized molecular chaperones and proteases (6). Mitochondria harbor an independent proteolytic system comprising of at least 45 proteases localized in different compartments of human mitochondria including the outer membrane, the intermembrane space, the inner membrane, and the mitochondrial matrix. The ClpXP complex (the serine protease ClpP and the AAA+ATPase ClpX), localized in the mitochondrial matrix, is one of these proteases. It digests inner membrane proteins including subunits of respiratory complexes and translocases, as well as proteins within the matrix. Much of our understanding of the structure and function of human ClpP stems from studies of the bacterial homolog and the crystal structure of human mitochondrial at 2.1 Å. Similar to the bacterial enzyme, mitochondrial ClpP is a large cylindrical tetradecamer composed of two identical stable heptameric rings enclosing a large aqueous chamber (6).

Each ClpP monomer has a compact body, called the “head region”, and an expanded α/β unit called the “handle region”. Heads of seven monomers build up the heptameric rings through hydrophobic interactions and the handles establish transient contacts to the adjacent heptameric ring through hydrogen bonds. The protease contains 14 internal catalytic cleavage sites and each subunit in the ClpP homotetradecamer harbors an active site with catalytic residues of Ser153, His178, and Asp227 (6).

Like bacterial ClpP, mitochondrial ClpP has three different conformational states: extended, compacted, and compressed. Among them, only the extended form demonstrates catalytic activity required for substrate degradation, while the others are supposed to be part of a barrel-opening cycle (6).

Mitochondrial ClpP lacks intrinsic ATPase activity and each subunit contains only the domain for digestion of small peptides (six or fewer amino acids) without ATP requirement. To get a processive proteolytic activity to degrade full-length proteins, human ClpP assembles into a tetradecamer in the presence of its ATPase, ClpX. In mammalian cells, ClpP forms a heterodimer with its ClpX chaperone, forming a macromolecular complex termed ClpXP. ClpX is a member

of the AAA+ protein superfamily, which includes ATPases associated with various cellular activities. This nuclear-encoded protein is the only known ATPase partner for mammalian ClpP. The substrate specificity of ClpXP is mediated by ClpX. Proteins destined for degradation by the ClpXP complex are recognized and unfolded by ClpX. Unfolded substrates are then fed into the lumen of ClpP's proteolytic chamber and degraded into small peptides fragments and probably expelled through the transient side pores (6).

The main function of mitochondrial ClpXP is to preserve protein quality control by degrading denatured or misfolded proteins. To date, several ClpXP substrates have been identified, including proteins involved in TCA cycle, electron transport, and other metabolic processes. By degrading misfolded or damaged respiratory chain proteins, ClpXP maintains the integrity of the respiratory chain and sustains OXPHOS (6).

ClpXP also plays a role in the mitochondrial unfolded protein response (UPRmt), a mitochondria-to-nucleus stress signalling pathway that decreases mitochondrial translation, adjusts cellular metabolism, and confers protection against pathogens. Most of the information regarding ClpXP's role in UPRmt stems from studies in *C*. elegans, but a similar pathway is likely to present in higher organisms (6).

Acute myeloid leukemia (AML) cells and stem cells, as well as subsets of other malignancies such as chronic myeloid leukemia (CML), pancreatic and breast cancer have unique mitochondrial characteristics with increased dependence on oxidative phosphorylation. The increased reliance on oxidative phosphorylation is due, at least in part, to increased flux of substrates into the TCA cycle, decreased spare reserve capacity, and inability to upmodulate other metabolic pathways upon suppression of oxidative phosphorylation. These data highlight a unique metabolic vulnerability and suggest that targeting OXPHOS could selectively kill these malignant cells. In particular, targeting ClpXP is an emerging anticancer strategy that exploits the increased dependence of OXPHOS in these cancers (6).

ClpP is overexpressed in subgroups of patients with multiple malignancies including AML, breast, lung, liver, ovary, prostate, uterus, stomach, testis, bladder, thyroid, and non-small cell lung cancer. ClpP expression is positively correlated with UPRmt gene signature. However, the direct regulators of

mammalian ClpP expression, such as transcription factors and epigenetic marks that lead to its dysregulated expression in cancer, have not been hitherto identified. Additionally, ClpX expression in cancer has not been widely reported. Further studies are also required to establish how ClpXP contributes to carcinogenesis. ClpP is necessary for the viability, growth, resistant, and metastasis of a subset of malignancies and perturbing ClpP with genetic or chemical approaches kills malignant cells with high ClpP expression. Consistent with its role in preserving the integrity of respiratory chain complexes, either loss or hyperactivation of ClpP increase ROS production, decrease respiratory chain complex activity, and impair OXPHOS, which appears functionally important for cell death after perturbing ClpP (6).

In contrast to the cytotoxic effects of inhibiting ClpP in cancer, normal cells are relatively insensitive to ClpP manipulation. ClpP is predominantly expressed in tissues with high mitochondrial content such as skeletal muscle, heart and liver (6). Despite its high expression in critical organs, ClpP knockout mice are viable, but slightly smaller than their wild type counterparts. ClpP −/− mice are also infertile and acquire hearing loss (7). In humans, rare individuals from consanguineous families have homozygous inactivating mutations in ClpP. These individuals also have acquired hearing loss and infertility (8). These studies support a therapeutic window for the development of drugs acting on ClpP for the treatment of several cancers.

1.3 The imipridones

Imipridones are a novel class of anti-cancer agents currently in phase I/II clinical trials for several advanced cancers. ONC201 is the founding member of this class of molecules that share a unique heterocyclic pharmacophore. ONC201 was discovered as a TRAIL gene inducing compound (TIC10) using a phenotypic, cell-based screen to identify compounds that upregulate TRAIL expression that would lead to TRAIL synthesis by tumor (and normal) cells in a p53-independent fashion (9). This screen was designed based on earlier studies that showed p53-dependent upmodulation of the TRAIL gene. The cell-based chemical library screen used a TRAIL gene promoter lacking p53 DNA-binding sites that was

linked to a luciferase reporter gene. The initial characterization of ONC201 showed that it inhibited ERK and Akt leading to Foxo3a translocation to the nucleus and TRAIL transcriptional activation. ONC201 demonstrated anti-tumor effects in numerous preclinical *in vivo* models (10). Subsequent work identified ONC201 as an activator of the integrated stress response (ISR) involving ATF4/CHOP and downstream activation of TRAIL receptor DR5. Upstream of ATF4, ONC201 appeared to signal through kinases HRI and PKR, eIF2-alpha and ATF4. Downstream of target engagement, ONC201 treatment leads to two outcomes: activation of the ISR pathway, which is also activated by proteasome inhibitors, and Akt/ERK inactivation, which is also caused by EGFR, Akt and RAF/MEK/ERK inhibitors (11). Thus, ISR activation is an early effect of ONC201 treatment that causes upmodulation of ATF4 translation and CHOP transcription in tumor cells within a few hours, whereas dual inactivation of Akt and ERK is a late effect, and cell death is also demonstrated to be quite slow, taking 2–3 days. These effects ultimately converge to induce the pro-apoptotic ligand TRAIL through activation and nuclear translocation of the transcription factor Foxo3a, as well as its receptor DR5, which may be induced by CHOP in addition to Foxo3a (10, 11). Additionally, ONC201 has been shown to degrade c-myc through a mechanism involving Akt/GSK3beta, which was demonstrated in glioma cell lines. Recently, the mitochondrial protease ClpP has been identified as the intracellular target for both ONC201 and its more potent, fluorinated derivative ONC212. ONC201 and ONC212 interact with human ClpP via non-covalent allosteric interactions that result in the protein complex opening specific areas of a substrate channel and altering the conformation of its active site. This imipridone-induced conformation causes hyperactivation of the enzymatic activity of ClpP, leading to increased degradation of respiratory chain complex subunits (12). These changes cause impaired OXPHOS that results in mitochondrial dysfunction and tumor cell killing. The underlying mechanisms and links between ClpP activation and the cellular pathways of cell death remain under investigation. Inactivating mutations in ClpP, as well as loss of ClpP expression, render leukemia and breast cancer cells partially resistant to imipridones, indicating that activation of ClpP is critical for its efficacy in these tumor types with a more

prominent contribution demonstrated in leukemic versus breast cancer cell lines (12). Mechanistically, ClpP activation triggers the UPRmt that can upregulate the ATF4/CHOP axis. Furthermore, disruption of mitochondrial function (e.g. OXPHOS) in cancer cells has been recently reported for ONC201, which may be explained by ClpP agonism (12). Whether ClpP expression or activity ultimately is sufficient to predict ONC201 sensitivity in humans is matter of ongoing investigation. There are numerous mechanisms for resistance to cell death within tumor cells, and so while expression of the ClpP target may be necessary for ONC201 sensitivity, it may not suffice to predict cell death in tumor cells.

2. AIMS OF THE STUDY

ONC212 is a fluorinated imipridone demonstrating more potent anti-cancer activity in the nM range as compared to the first-in-class molecule ONC201 that is active in the low μM range (13, 14). Despite initially being discovered as TRAIL-inducing compounds (15), imipridones hinder tumor growth through a more complex, often cell context-dependent, mechanism (9). In solid cancers, they promote growth arrest and extrinsic apoptosis through the induction of the integrated stress response and upregulation of TRAIL/DR5 (10, 11). In addition, they act as synthetic ligands for specific G protein-coupled receptors often overexpressed on cancer cells, thus modulating cAMP-dependent signaling pathways that ultimately impact cell viability (16, 17). More recently, the mitochondrial peptidase ClpP has been identified as a novel intracellular target for both ONC201 and ONC212 (18). Imipridones dock directly into the hydrophobic pocket of the ClpP subunit, causing its enzymatic hyperactivation (18). Because many components of the respiratory chain complexes are putative ClpP substrates, ONC201 and ONC212 dysregulate the turnover of key enzymes involved in OXPHOS, irreversibly undermining critical aspects of mitochondrial metabolism (18-20).

Although historically recognized as a highly glycolytic tumor, pancreatic adenocarcinoma needs functional mitochondria to meet its energy demands (21–23). The oncogenic mitogen-activated protein kinase (MAPK) pathway, constitutively activated in pancreatic cancer, contributes to the regulation of mitochondrial dynamics, while mitochondrial respiration, in turn, provides the amount of adenosine triphosphate (ATP) needed to sustain cell growth and proliferation, especially under low glucose availability (21, 22). Even if a peculiar metabolic reliance may occur in specific cell types, OXPHOS and glycolysis usually cooperate to make cancer cells metabolically plastic, a kind of paradigm in cancer biology accounting for the failure of some targeted agents when administered as monotherapy (24).

The aim of this study was to examine the impact of ONC212 on the bioenergetic profile of pancreatic cancer cells. Particularly, we investigated if ONC212 could

alter the expression of ClpP and ClpX, and if it could compromise oxidative phosphorylation. In addition, we correlated ONC212 sensitivity to the metabolic profile of cancer cells to find out metabolic biomarkers potentially predicting *in vitro* response to ONC212. Lastly, we evaluated *in vitro* and *in vivo* if glycolysis could favor the escape of pancreatic cancer cells from ONC212-triggered apoptosis.

Overall, we found that mitochondrial metabolism is invariably suppressed upon ONC212 treatment, but the cellular outcomes actually differ based on divergent metabolic dependencies.

3. MATERIALS AND METHODS

3.1 Cell cultures and reagents

All pancreatic cancer cell lines were purchased from American Type Culture Collection (ATCC). The cell lines were maintained in high glucose DMEM supplemented with glutamine 2 mM, pyruvate 1 mM, non-essential amino acids 1X (all from Thermo Fisher Scientific, Waltham, MA, USA), 10% fetal bovine serum (FBS) and 1% penicillin-streptomycin (Cornig, NY, USA, Cat no. 30-002-CI) (complete medium, CM). In selected experiments, cells were cultured in no glucose DMEM (Thermo Fisher Scientific, Cat no. 11966025), supplemented with galactose 20 mM (Sigma Aldrich, St. Louis, MO, USA, Cat no. G5388), glutamine 2 mM, pyruvate 1 mM, non-essential amino acids 1X, 10% FBS and 1% penicillin-streptomycin. Cell lines were authenticated routinely and mycoplasma free. ONC212 was obtained from Oncoceutics, Inc (Philadelphia, PA, USA). MG132 was purchased from Selleckchem (Houston, TX, USA, Cat no. S2619), epoxomicin and bafilomycin A1 from Sigma-Aldrich (Cat no. E3652 and B1793, respectively). 2-deoxy-D-glucose (2-DG) was obtained from Sigma-Aldrich (Cat no. D6134).

3.2 Cell viability assay and synergy assessment

Cell viability was measured by CellTiter-Glo (CTG, Promega, Madison, WI, Cat no. G7572). Briefly, $5x10^3$ cells/well were seeded overnight in a 96-well plate at 37°C and 5% CO_2. In selected experiments, the hypoxic environment (0.5–1% O_2) was created using the INVIVO2 hypoxia workstation (TOUCAN Technologies). Cells were treated with either single agent or combination of ONC212 and 2-DG, at indicated concentrations. After 72 hours, luminescent-based cell viability was determined using CTG assay, following the manufacturer's instructions. Percent of cell viability was determined by normalizing luminescence signal to control wells. Results were reported as % viability ± standard deviation (SD). Dose-response curves were generated and the half-maximal growth inhibition concentration (GI50) was calculated using GraphPad Prism version 7 (La Jolla, CA, USA). Compusyn software (ComboSyn, Inc.) was used to calculate the

combination indices (CI). CI < 1 indicates some degree of synergy. CI < 0.5 indicates a very strong synergy.

3.3 Immunoblotting

Cells were seeded in a 6-well plate at a density of $5x10^5$ cells/well and left to adhere overnight. Treatment with either vehicle or ONC212 at the indicated concentrations was added for the indicated time. At the end of culture, cells were mechanically detached, washed with PBS and lysed with RIPA buffer (Sigma Aldrich, Cat no. R0278) supplemented with protease inhibitor (Sigma Aldrich, Cat no. 4693159001). Protein concentration was determined using BCA Protein Assay Kit (Thermo Fisher Scientific, Cat no. 23223). After boiling the protein samples in sample buffer (Thermo Fisher Scientific, Cat no. LC2673), equal amounts of proteins were loaded onto NuPAGE 4-12% Bis-Tris gel (Thermo Fisher Scientific, Cat no. NP0323). After electrophoresis, proteins were transferred to a polyvinylidene difluoride (PVDF) membrane. After blocking with TBST with 5% w/v nonfat dry milk, the membranes were incubated with primary antibody overnight at 4°C. Afterwards, membranes were incubated for 45 minutes at room temperature with the appropriate secondary antibodies, labeled with horseradish peroxidase. Chemiluminescence reaction was detected using the ECL Reagent (Thermo Fisher Scientific, Cat no. 32106). Ran or β-actin was used as loading control. Antibodies used in this study were listed in Table 1.

3.4 siRNA transfection

Cells were plated in medium without antibiotics and incubated overnight. siRNA targeting ClpP (Santa Cruz Biotechnology, Dallas, TX, USA, Cat no. sc-60413) or AMPK (Santa Cruz Biotechnology, Cat no. sc-45312), or control siRNA (Quiagen, Hilden, DE, Cat no. 1022076) were transfected into cells using Lipofectamine RNAiMax (Life Technologies, Carlsbad, CA, USA, Cat no. 13778075), following the manufacturer's instructions. After 48 hours, cells were treated with vehicle (dimethyl sulfoxide, DMSO) or ONC212 for an additional 24 hours (WB experiments) or 72 hours (CTG experiments). Western blot was performed to assess the level of knockdown.

3.5 Extracellular lactate measurement

Cells were seeded in a 96 well plate at a density of $1x10^4$ cells/well. Extracellular lactate was measured in the cell culture supernatant after 24 or 48 hours of treatment with DMSO or ONC212 at the indicated dosages. The Lactate-Glo assay kit (Promega, Cat no. J5021) was used, according to the manufacturer's instructions. Bioluminescence was measured by a microplate luminometer and data were normalized to cell viability, as measured by the CTG assay. Results were presented as lactate relative light units (RLU)/cells RLU.

3.6 NAD^+/NADH determination

Cells cultured in CM without pyruvate supplementation were seeded in a 96 well plate at a density of $4x10^4$ cells/well and treated with DMSO or ONC212 at the indicated concentrations. After 24 hours, NAD^+ and NADH levels were individually assessed in cell lysates using the NAD^+/NADH-Glo assay kit (Promega, Cat no. G9071), following manufacturer's protocol. Results were represented as NAD^+/NADH ratio.

3.7 Immunofluorescence staining

Cells were seeded in 8-well chamber slides (Thermo Fisher Scientific, Cat no. 154941PK) at a density of $3x10^4$ cells/well and were treated with DMSO or ONC212 for 24 hours. After removing the culture media, cell fixation and permeabilization were achieved using the following protocol: incubation with fixation/permeabilization solution (BD Biosciences, San Jose, CA, USA, Cat no. 554722) for 30 min, perm/wash buffer (BD Biosciences, Cat no. 554723) for 30 min, TBST buffer for 30 min. Blocking was performed by incubating cells with donkey serum 2.5% in perm/wash buffer. Cells were incubated overnight at 4°C with primary antibodies (Table 1) diluted 1:200 in blocking buffer. After washing, goat anti-mouse or anti-rabbit secondary antibodies conjugated to Cy3 or Alexa-488, respectively, were added and left to incubate for 2 hours at room temperature. After washing, cells were counterstained with DAPI and imaged by an Inverted Zeiss LSM 880 confocal microscope.

3.8 Extracellular flux analysis

5 x 10^4 cells were seeded on XF96 cell culture microplates (Agilent Technologies Inc., Wilmington, DE, USA). After 24 hours, cells were treated with DMSO or ONC212 at the indicated concentrations for an additional 48 hours. Then the ATP Real-Time rate assay (Agilent Technologies Inc., Cat no. 103592-100) was performed on an Agilent Seahorse XFe96 analyzer, as described by the manufacturer. The ATP rate assay contains 10 mM of XF glucose, 1 mM of XF pyruvate, and 2 mM of XF glutamine. Serial injections of DMSO or ONC212 (port 1, final concentration 0.2 or 0.4 μM), oligomycin (port 2, final concentration 1.5 μM) and rotenone/antimycin A (Rot/AA, port 3, final concentration 0.5 μM) were applied. Oxygen consumption rate (OCR, pmol/min) and extracellular acidification rate (ECAR, mpH/min) were dynamically measured by the instrument. Proton efflux rate (PER, pmol H^+/min), OCR_{ATP} (i.e. the rate of oxygen consumption that is coupled to ATP production during OXPHOS), mitochondria-derived ATP production rate (mitoATP, pmol ATP/min), mitochondrial PER (mitoPER), glycolytic PER (glycoPER) and glycolysis-derived ATP production rate (glycoATP) were calculated as follows: PER = ECAR x buffer factor (mmol/L/pH) x Vol measurement chamber (μL) x scaling factor (Kvol); OCR_{ATP} = OCR - OCR_{Oligo}; mitoATP = OCR_{ATP} x 2 (pmol O/pmol O_2) x 2.75; mitoPER = PER_{basal} – $PER_{Rot/AA}$; glycoPER = PER – mitoPER; glycoATP = glycoPER. Data were processed with Wave software.

3.9 *In vivo* studies

The experimental *in vivo* protocol was approved by the Institutional Animal Care and Use Committee (IACUC) of Brown University. Six- to seven-week old female nu/nu athymic mice were purchased from Taconic (Hudson, NY, USA). For the short-term experiment, 5 x 10^6 BxPC3 or HPAF-II cells were suspended in 50 μL PBS mixed with 50 μL Matrigel (Thermo Fisher Scientific, Cat no. 354234), and injected subcutaneously into the rear flanks of 24 mice. Once tumor volume reached at least 100 mm^3, mice were randomly assigned to one of four groups (3 mice/group): vehicle, ONC212, 2-DG, combination of ONC212 + 2-

DG. ONC212 was delivered by oral gavage at the dosage of 50 mg/Kg in a solution of 70% PBS, 10% DMSO and 20% Kolliphor EL (Sigma Aldrich, Cat no. C5135), three times per week. 2-DG was administered by intraperitoneal injection at the dosage of 500 mg/Kg diluted in PBS, three times per week. Mice were sacrificed after one week of treatment (= 3 doses) for biomarker analyses (immunohistochemistry (IHC) and blood tests). For the long-term experiment, 5 x 10^6 BxPC3 cells were injected in 24 mice following the same procedure as described above. Once tumor volume reached at least 100 mm^3, mice were randomly assigned to vehicle, ONC212, 2-DG, or the combination of ONC212 + 2-DG, administered three times per week at the same dosage as reported above. The treatment continued until mice developed signs of toxicity or discomfort from excessive tumor growth. Mice were weighed once a week to monitor signs of drug toxicity. The length (L) and width (W) of the masses were measured 3 times/week with a digital caliper, and the tumor volume was calculated applying the formula: 0.5*L*W^2. The analyses of tumor growth were limited to the mice starting treatment with a tumor volume of 100-250 mm^3 (vehicle = 4; ONC212 = 6; 2-DG = 4; combination = 5). Collection of whole blood and serum were performed by cardiac puncture and sent to Antech GLP (Morrisville, NC, USA) for blood cell count and chemistry tests. Tumors and organs were dissected and harvested for IHC.

3.10 Immunohistochemistry

Excised tumors were fixed in formalin. Paraffin embedding and sectioning of slides were performed by the Brown University Molecular Pathology Core Facility. Slides were de-waxed in xylene and subsequently hydrated in ethanol at decreasing concentrations. Antigen retrieval was carried out by boiling the slides in 2.1 g citric acid (pH 6) for 10 min. Endogenous peroxidase were quenched by incubating the slides in 3% hydrogen peroxide for 5 min. After nuclear membrane permeabilization with TBS-T, slides were blocked with horse serum (Vector Laboratories, San Francisco, CA, USA, Cat no. MP-7401-15), and incubated with primary antibodies overnight (Table 1) in a humidified chamber at 4°C. After washing with PBS, secondary antibody (Vector Laboratories, Cat no. MP-7401-15

or MP-7402) was added for 30 minutes, followed by DAB application (Thermo Fisher Scientific, Cat no. NC9276270), according to the manufacturer's protocol. Samples were counterstained with haematoxylin, rinsed with distilled water, dehydrated in an increasing gradient of ethanol, cleared with xylene, and mounted with Cytoseal mounting medium (Thermo Fisher Scientific, Cat no. 8312-4). Images were recorded on an Axioskop microscope (Zeiss), using QCapture. QuPath software was used to automatically count positive cells (25). For each IHC marker, 5 20x images per group were analyzed, and results were represented as the absolute number of positive cells per 20x field (26).

3.11 Statistics

Statistical analyses were conducted using GraphPad Prism 7. The Student's two-tailed T test was used for pairwise analysis. Data are presented as means ± standard deviation (SD) from at least 3 independent experiments, unless otherwise specified. Differences were considered significant for p values <0.05.

Table 1. List of antibodies used in this study for western blots (WB), immunofluorescence (IF) and immunohistochemistry (IHC).

Antibody	Cat. no	Source
ClpP (WB, IF)	sc-271284	Santa Cruz
ClpX (WB, IF)	ab168338	Abcam
Ran (WB)	610341	BD Biosciences
AMPK (WB)	2532S	Cell Signaling
pAMPK (WB)	2535S	Cell Signaling
pERK (WB, IHC)	4370	Cell Signaling
ERK (WB)	9102S	Cell Signaling
cPARP (WB)	9546s	Cell Signaling
GLUT1 (WB)	sc-377228	Santa Cruz
GLUT4 (WB)	sc-53566	Santa Cruz
SDH-A (WB)	5839S	Cell Signaling
SDH-B (WB)	ab14714	Abcam
NDUFA12 (WB)	ab192617	Abcam
COXIV (WB)	4850S	Cell Signaling
LDH-A (WB)	3582S	Cell Signaling
HK2 (WB)	2867S	Cell Signaling
Actin (WB)	sc-8432	Santa Cruz
TOM20 (WB, IF)	42406	Cell Signaling
Tubulin (WB)	2144S	Cell Signaling
Ki 67 (IHC)	9449S	Cell Signaling
ClpX (IHC)	HPA040262	Sigma Aldrich
cc3 (IHC)	9661S	Cell Signaling

4. RESULTS

4.1 The ClpXP complex is disrupted by ONC212 in pancreatic cancer cells

Although the ClpXP complex is often detected at the protein level in human cancers (19) and normal cells (Fig. 1A), its expression in the specific context of pancreatic cancer has not been hitherto studied. Moreover, it is uncertain if the imipridone-induced ClpP hyperactivation, first described in blood cancers and a few solid tumor types (18, 27, 28), can be generalized to other malignancies. We analyzed ClpP and ClpX expression in a panel of pancreatic cancer cell lines, and assessed if ONC212 treatment could provoke ClpX suppression, a marker of uncontrolled ClpP activity (27, 29). We found that both ClpP and ClpX are highly expressed across all pancreatic cancer cell lines tested (Fig. 1B-E).

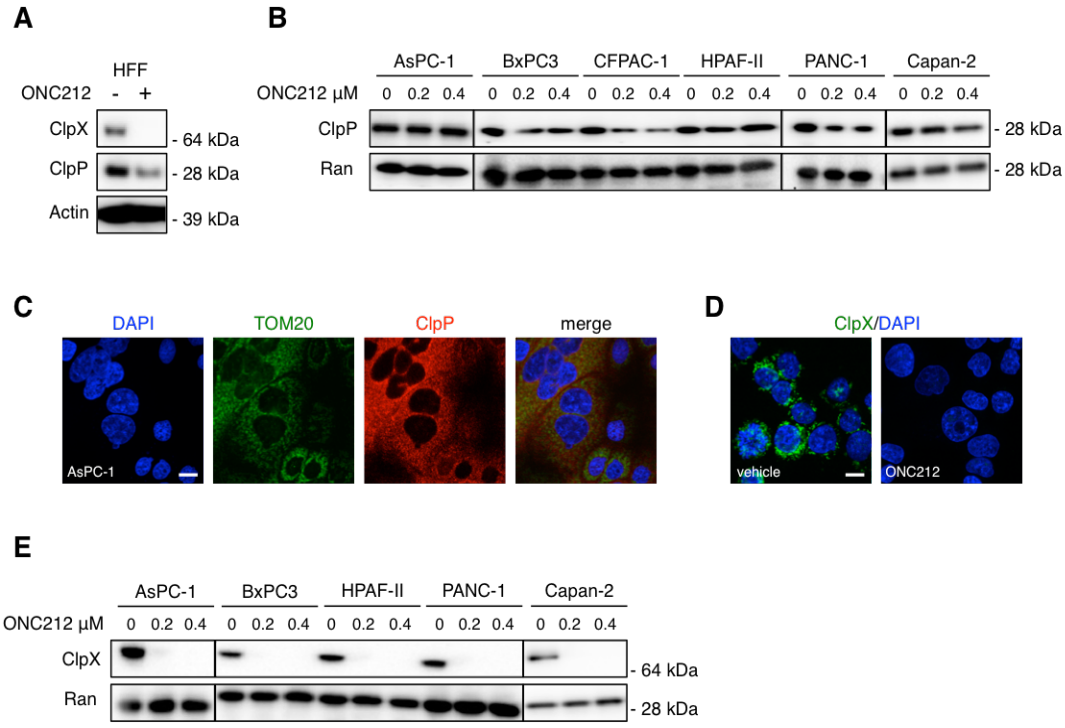

Figure 1. ClpXP expression in pancreatic cancer cell lines. (A) Western blot analysis for ClpX and ClpP expression in normal human fibroblasts (HFF cell line) treated or not with 1 µM ONC212 for 48 hours. (B) Western blot analysis for ClpP was performed in the indicated pancreatic cancer cell lines treated or not with ONC212 for 48 hours. (C) Immunofluorescence detection of ClpP (Cy3) in AsPC1 cells, showing its co-localization with the mitochondrial marker TOM20 (Alexa Fluor 488). Sample was counterstained with DAPI and visualized by confocal microscopy. Magnification 63x. Scale bar: 6 µm. (D) Immunofluorescence analysis of ClpX (Alexa Fluor 488) in BxPC3 cells treated or not with 0.2 µM ONC212 for 24 hours. Magnification: 100x. Scale bar: 9 µm. (E) Western blot analysis for ClpX in the indicated cell lines treated or not with ONC212 for 48h.

ONC212 treatment, at doses comparable to the previously reported growth inhibitory concentration (GI50) values (30), caused a slight, if any, reduction of ClpP protein level after 48 hours (Fig. 1B). Conversely, ClpX expression was abolished by the treatment (Fig. 1D, E).

Kinetic analysis showed that ONC212 reduced ClpX expression in a time-dependent manner, with an almost complete suppression as soon as 6 hours after treatment (Fig. 2A). Nude mice xenografted with BxPC3 or HPAF-II cells had reduced ClpX expression in the tumor mass after short-term treatment with ONC212 (Fig. 2B, C). Also human foreskin fibroblasts (HFF cell lines) had decreased ClpX expression in response to ONC212 (Fig. 1A). *In vitro* co-treatment with the proteasome inhibitors MG132 or epoxomicin did not prevent ONC212-induced ClpX downregulation. The autophagy inhibitor bafilomycin A1 was not able to rescue ClpX expression either (Fig. 2D). Instead, ClpP knockdown restored ClpX expression in cells treated with ONC212, suggesting ClpP is required for ONC212-triggered ClpX suppression (Fig. 2E). Therefore, ONC212 disrupted the ClpXP complex and rapidly promoted the acquisition of a $ClpX^{neg}ClpP^{pos}$ phenotype, which is consistent with compounds that confer uncontrolled proteolytic capacity on ClpP (27, 29). To confirm that ClpP hyperactivation plays a role in the antitumor activity of ONC212 against pancreatic cancer, we performed knockdown experiments on multiple cell lines. As expected, ClpP downregulation by specific siRNA partially compromised the growth inhibitory effect of ONC212 in the Capan-2, HPAF-II and BxPC3 cells (Fig. 3A). Interestingly, in the absence of any treatment, the viability of ClpP-knockdown HPAF-II and BxPC3 cells was higher as compared to controls (Fig. 3B). While this contrasts with data from AML and prostate carcinoma, where ClpP knockdown impairs cell growth (19, 31), it is in keeping with pancreatic cancer TCGA transcriptomic results showing a positive correlation between ClpP expression and favorable prognosis (32).

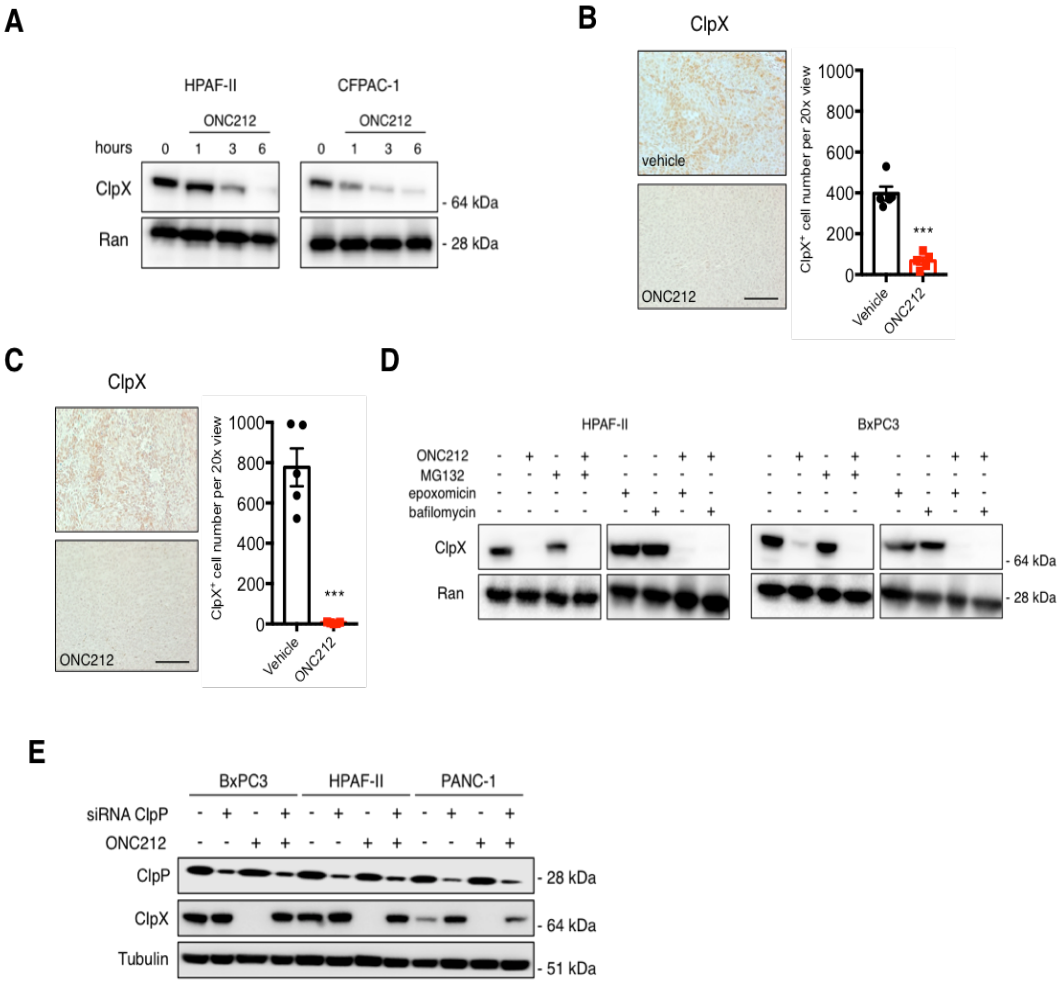

Figure 2. ONC212 suppresses ClpX expression. (A) Kinetic western blot showing the downregulation of ClpX in cells treated with 0.2 µM ONC212 for up to 6 hours. **(B)** IHC staining of ClpX in BxPC3 xenografts treated with 3 doses of vehicle or ONC212. Images were captured at 20x magnification. Scale bar: 100 µm. Data are expressed as mean ± SEM. ***p<0.001 **(C)** IHC staining of ClpX in HPAF-II xenografts treated with 3 doses of vehicle or ONC212. Images were captured at 20x magnification. Scale bar: 100 µm. Data are expressed as mean ± SEM. ***p<0.001 **(D)** Western blot analysis for ClpX in HPAF-II and BxPC3 cells treated or not with ONC212 and the indicated inhibitors for 6 hours. **(E)** The indicated cell lines were transfected with scrambled siRNA ClpP-specific siRNA (siClpP). After 24 hours, cells were treated with 0.2 µM ONC212 for an additional 24 hours. Western blot analysis for ClpP and ClpX was performed.

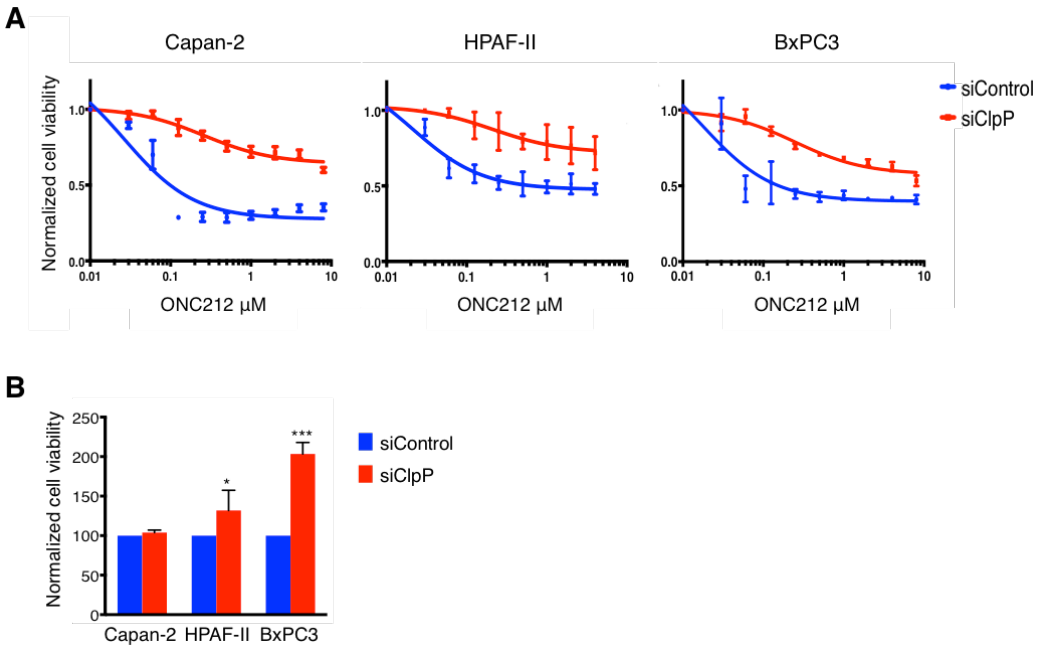

Figure 3. ClpP is required for ONC212 activity. (A) The indicated cell lines were transfected with scrambled siRNA (siControl) or ClpP-specific siRNA (siClpP). After 48 hours, cells were treated with ONC212 for an additional 72 hours. Afterwards, cell viability was assessed by CTG assay. Dose-response curves summarizing results from three independent experiments are shown. **(B)** Cell viability assessed by CTG assay 48 hours after transfection with siControl or siClpP. Results were normalized to siControl cells. Means (columns) of three independent experiments and SD (bars) are represented. *p<0.05, ***p<0.001.

4.2 ONC212 impairs mitochondrial bioenergetics

Several mitochondrial proteins involved in OXPHOS, Kreb's cycle and mitochondrial translation have been identified as putative substrates of ClpP (18, 31). We focused on the OXPHOS machinery and addressed whether ONC212-induced ClpP hyperactivation could decrease the expression of key enzymes belonging to respiratory chain complexes. We found that NADH:ubiquinone oxidoreductase subunit A12 (NDUFA12, complex I), succinate dehydrogenase subunit A (SDH-A, complex II) and succinate dehydrogenase subunit B (SDH-B, complex II) were downregulated following 48 hours of treatment with ONC212 (Fig. 4A). This was consistent across all cancer cell lines, although the degree of protein downregulation was not identical, with HPAF-II and PANC-1 cells showing the most evident protein decrease. CFPAC-1 and Capan-2 cells were also tested at a shorter time point and showed similar protein suppression (Fig. 4B), suggesting that ONC212 affects the electron transport chain early on. Cytochrome C oxidase subunit IV (COXIV, belonging to complex IV) expression was also

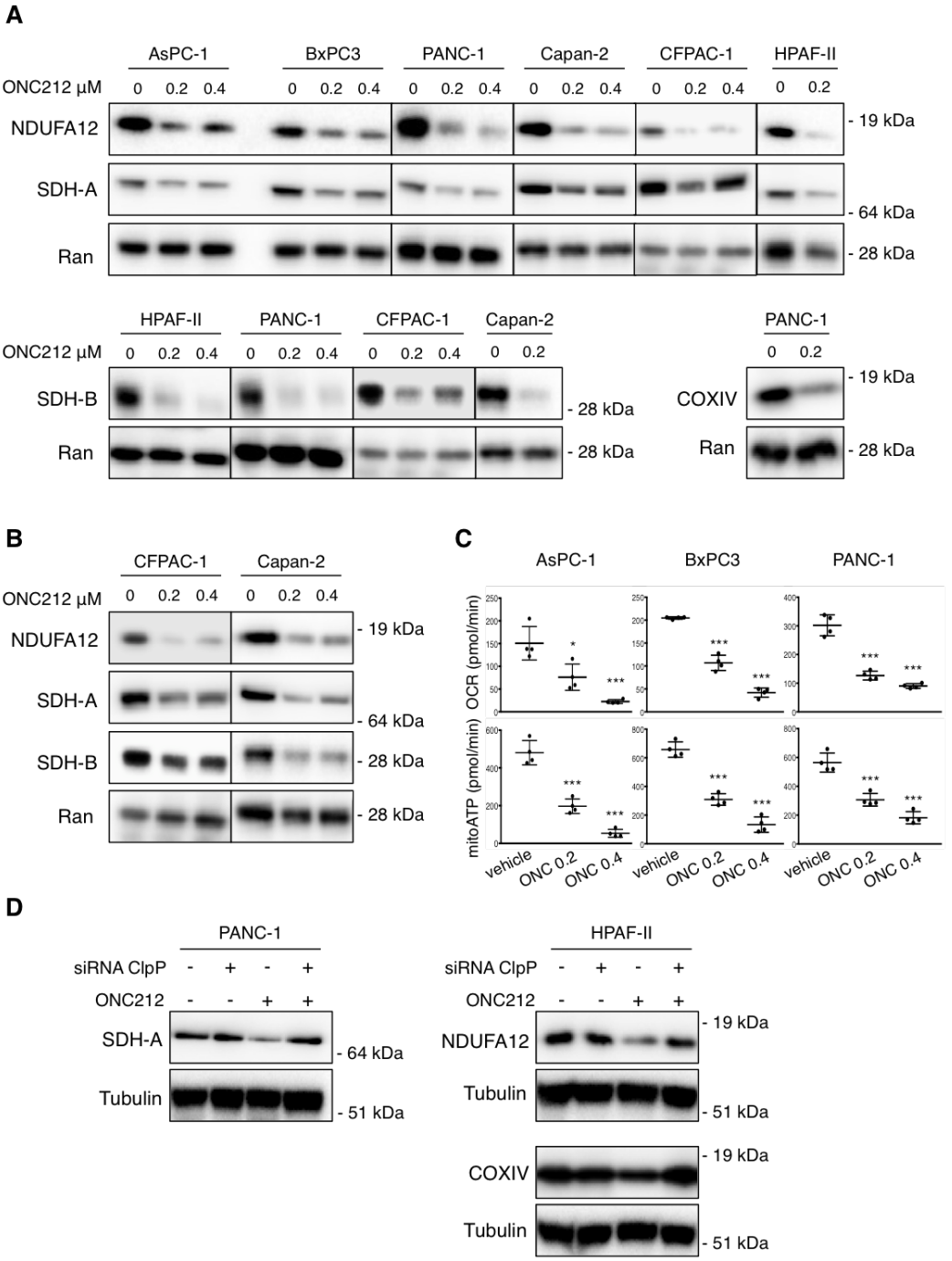

Figure 4. ONC212 inhibits OXPHOS. (A) Western blot analysis for NDUFA12, SDH-A, SDH-B and COXIV in the indicated cell lines treated or not with ONC212 for 48 hours. **(B)** Western blot for NDUFA12, SDH-A and SDH-B in CFPAC-1 and Capan-2 cells treated with the indicated doses of ONC212 for 24 hours. Blots in (A) and (B) are representative of three independent experiments. **(C)** AsPC-1, BxPC3 and PANC-1 cells were treated for 48 hours with 0.2 or 0.4 µM ONC212 (ONC) prior to performing the ATP Real-Time rate assay. Continuous extracellular flux analysis was conducted to record basal OCR (upper panels) and calculate basal mitochondrial ATP production rate (mitoATP) (lower panels). **(D)** The same lysates as in Fig. 2E were probed for SDH-A, NDUFA12 and COX-IV. Data are expressed as mean ± SD. *p<0.05, ***p<0.001.

decreased by ONC212 in PANC-1 cells (Fig. 4A). We next performed extracellular flux analysis to determine if OXPHOS enzyme downregulation might lead to mitochondrial functional impairment. ONC212 treatment decreased basal OCR in a dose-dependent fashion, uniformly across the cell lines tested (AsPC-1, BxPC3 and PANC-1) (Fig. 4C). As a consequence, mitochondria-derived ATP production rate (mitoATP) remarkably dropped with ONC212 treatment (Fig. 4C). ClpP knockdown partially prevented the downregulation of OXPHOS proteins induced by ONC212 (Fig. 4D). The AMP-activated protein kinase (AMPK), a well-known molecular sensor of low energy status (33), is consequently phosphorylated at Thr172, with the exception of PANC-1 cells showing its constitutive activation (Fig. 5A). Knockdown of AMPK decreased the viability of PANC-1 cells (Fig. 5B, C) and enhanced their sensitivity to ONC212 (Fig. 5D). Although AMPK activation might play a protective role in PANC-1 cells, the relevance of this mechanism appears cell-context dependent as AMPK knockdown in BxPC3 cells does not influence the sensitivity to ONC212 (Fig. 5E).

4.3 Variable ONC212 sensitivity across pancreatic cancer cell lines

Given that OXPHOS inhibition occurred uniformly across all cancer cell lines upon ONC212 treatment, we wondered if its cytotoxic effect was similar among them. Cell viability assays performed after a 72-hour treatment period revealed that the cancer cell lines displayed different sensitivities to ONC212, with GI50 values ranging from 0.09 to 0.47 μM. AsPC-1 and HPAF-II were the most sensitive, with GI50 of 0.09 and 0.11 μM, respectively (Fig. 6A). Although we used the ATP-based CTG assay to measure cell viability, which could have overestimated the anti-proliferative effect of ONC212, our results are comparable to those reported in our previous study where orthogonal methods were used (30). Importantly, AsPC-1 and HPAF-II underwent apoptosis upon treatment with 0.2 and 0.4 μM ONC212, as demonstrated by the induction of poly (ADP-ribose) polymerase (PARP) cleavage. By contrast, all other cell lines did not show any PARP cleavage in response to ONC212, indicating that, in some cells, the

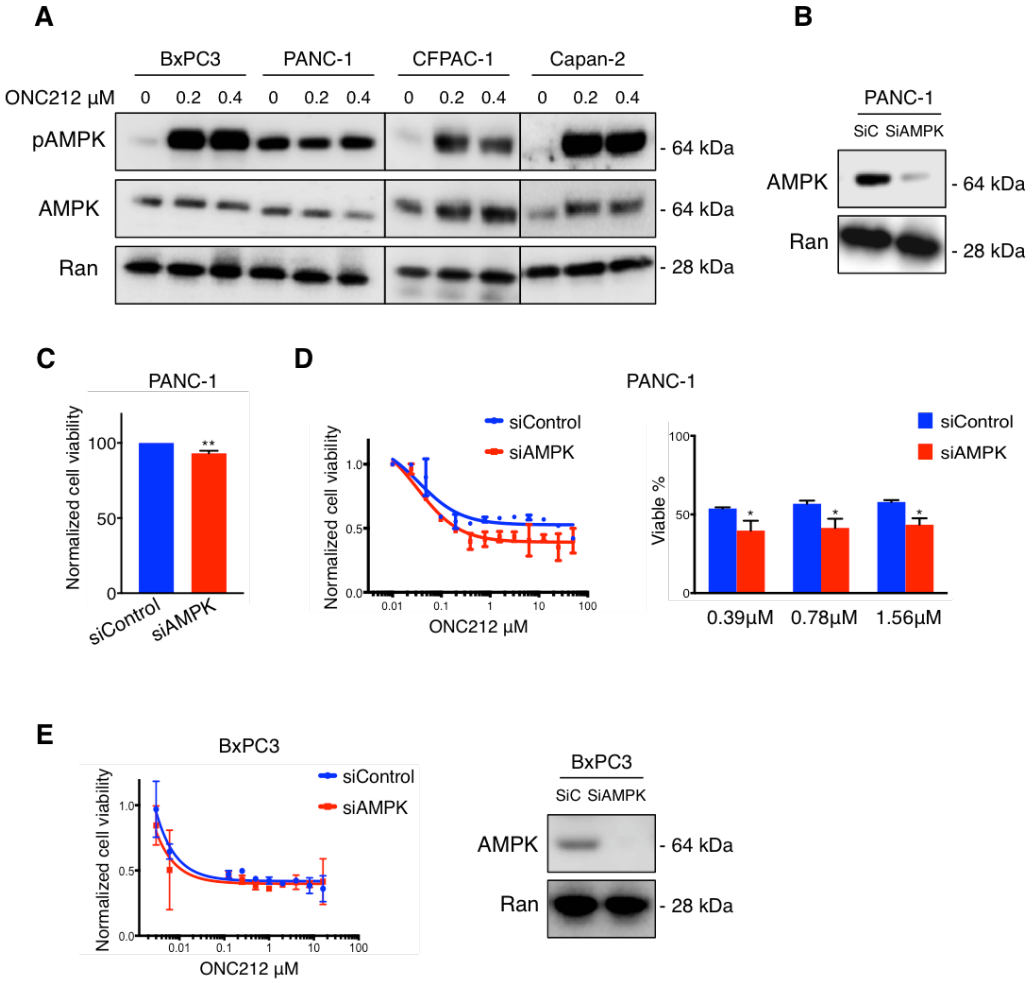

Figure 5. ONC212 triggers AMPK activation. (A) Western blot analysis for p-AMPK (Thr172) and AMPK in the indicated cell lines treated or not with ONC212 for 48 hours. Blots are representative of three independent experiments. **(B)** Western blot analysis for AMPK expression in PANC-1 cells transfected with scramble siRNA (siC) or AMPK-specific siRNA (siAMPK) for 48 hours. **(C)** PANC-1 cells were transfected with scramble siRNA (siControl) or siAMPK for 48 hours. Cell viability was assessed by CTG assay and plotted after normalization to siControl. N = 6 independent experiments. Data are expressed as mean ± SD. **p<0.001. **(D)** PANC1 cells were transfected with siControl or siAMPK for 48 hours and treated with ONC212 for an additional 72 hours. Afterwards, cell viability was assessed by CTG assay. *Left panel*. Dose-response curves summarizing the results from three independent experiments are shown (left panel). *Right panel*. Percentage of viable cells after treatment with ONC212 at the indicated concentrations. Comparison between siControl and siAMPK cells. Data are expressed as mean ± SD. N = 3 independent experiments. *p<0.05. **(E)** *Left panel*. Cell viability as assessed by CTG assay in BxPC3 cells transfected with either siControl or siAMPK for 48 hours and treated with ONC212 for an additional 72 hours. *Right panel*. Western blot analysis for AMPK expression in BxPC3 cells transfected with scramble siC or siAMPK for 48 hours.

ONC212 effect was likely limited to growth inhibition, with no apoptotic triggering (Fig. 6B). Extracellular signal-regulated kinase 1/2 (ERK1/2) phosphorylation, a hallmark of pancreatic cancer due to constitutive Ras mutation (34) and a previously described imipridones' downstream target (5), was affected

similarly: while ONC212 inhibited ERK1/2 in the most sensitive cells, it turned out to be ineffective in the less sensitive ones (Fig. 6C). Therefore, ONC212 sensitivity paralleled ERK1/2 inhibition and PARP cleavage. Although ClpP expression and OXPHOS inhibition were shared across all ONC212-treated cell lines, some of them were eventually killed while others were just growth-arrested.

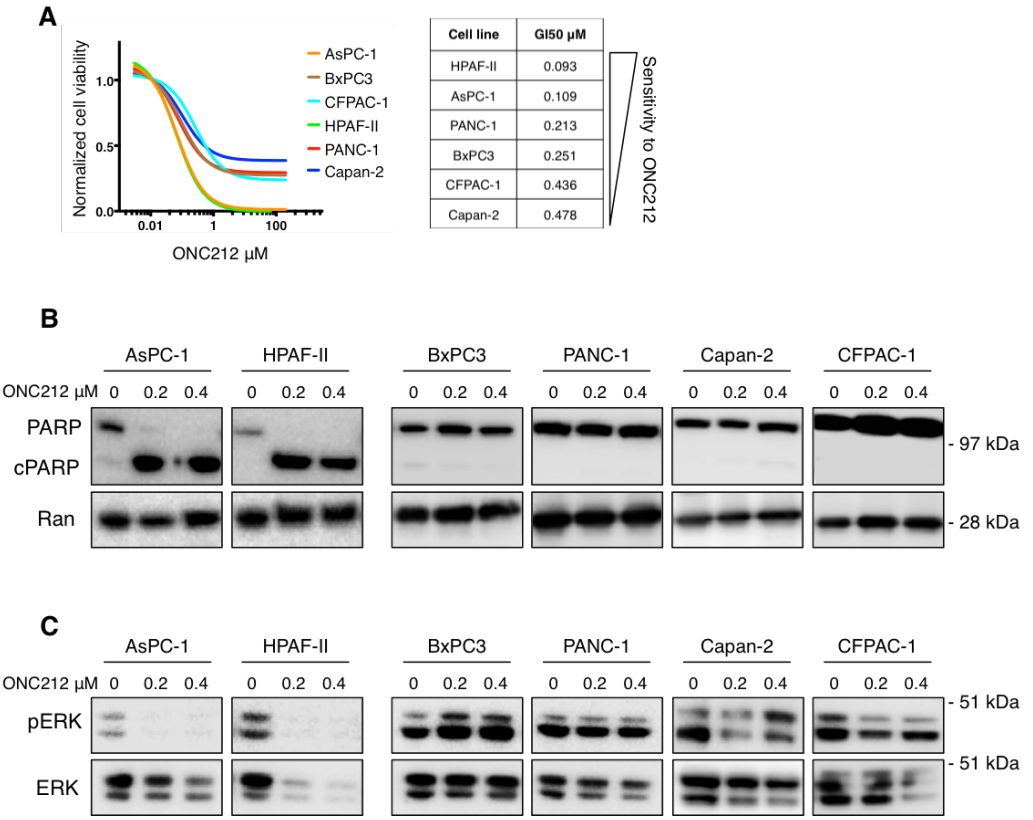

Figure 6. The antineoplastic effect of ONC212 is cell-context dependent. (A) The indicated cancer cell lines were treated with ONC212 for 72 hours. Cell viability was assessed by CTG assay. Dose-response curves are shown and GI50 values are summarized according to ONC212 sensitivity. **(B)** Western blot analysis for PARP cleavage in the indicated cell lines treated or not with ONC212 for 48 hours. **(C)** Western blot analysis for ERK phosphorylation in the indicated cell lines treated or not with ONC212 for 48 hours. Blots are representative of at least three independent experiments.

4.4 Glycolysis is boosted in ONC212-treated cell lines not undergoing apoptosis

Given the different cellular outcomes despite the same mitochondrial-impairing mechanism, we reasoned that cell-intrinsic metabolic features could tune the cytotoxic program of ONC212. Specifically, we focused on aerobic glycolysis, a major metabolic pathway supplying rapid ATP production and considered a

possible escape mechanism from cancer therapeutics (35, 36). In BxPC3 and PANC-1 cells, representative of the 'non-apoptotic' subgroup, the glycolytic rate as measured by glycoPER was significantly upregulated in response to a 48-hour treatment with ONC212 (Fig. 7A). As a result, the glycolysis-derived ATP production rate (glycoATP) increased and contributed to maintaining an acceptable amount of total ATP (Fig. 7B). Also, oligomycin injection did not further increase the glycolytic rate in ONC212-treated cells, suggesting the cell glycolytic capacity already reached its maximum (Fig. 8A). In stark contrast, AsPC1 cells, which usually die by apoptosis under ONC212, failed to sustain glycolysis and their glycoPER dramatically dropped, thus suffering a profound decline in ATP production (Fig. 7A, B). The upregulation of the glycolytic pathway in the less sensitive cell lines was further supported by the increased extracellular lactate concentration observed after ONC212 treatment in a time- and dose-dependent manner (Fig. 7C). Furthermore, in BxPC3 cells ONC212 perturbed the NAD^+/NADH ratio in favor of NAD^+, an essential cofactor fueling the glycolytic flux (Fig. 7D). In search of enzymes possibly involved in the glycolytic switch, we found that hexokinase II (HK II), catalyzing the phosphorylation of glucose to glucose-6-phosphate, was upregulated in response to ONC212 both in BxPC3 and PANC-1 cells. The glucose transporter GLUT1 increased in BxPC3 cells after treatment, while PANC-1 did not express it. Lactate dehydrogenase A (LDHA) was expressed in both cell lines without significant changes after treatment (Fig. 8B).

Collectively, ONC212 affected the metabolic profiles in a cell-context dependent manner. BxPC3 and PANC-1 cells, typically resistant to ONC212-induced apoptosis, became less oxidative but highly glycolytic. On the contrary, bioenergetics of the most sensitive AsPC-1 cells was completely turned off by the treatment, due to their inability to sustain glycolysis (Fig. 7E).

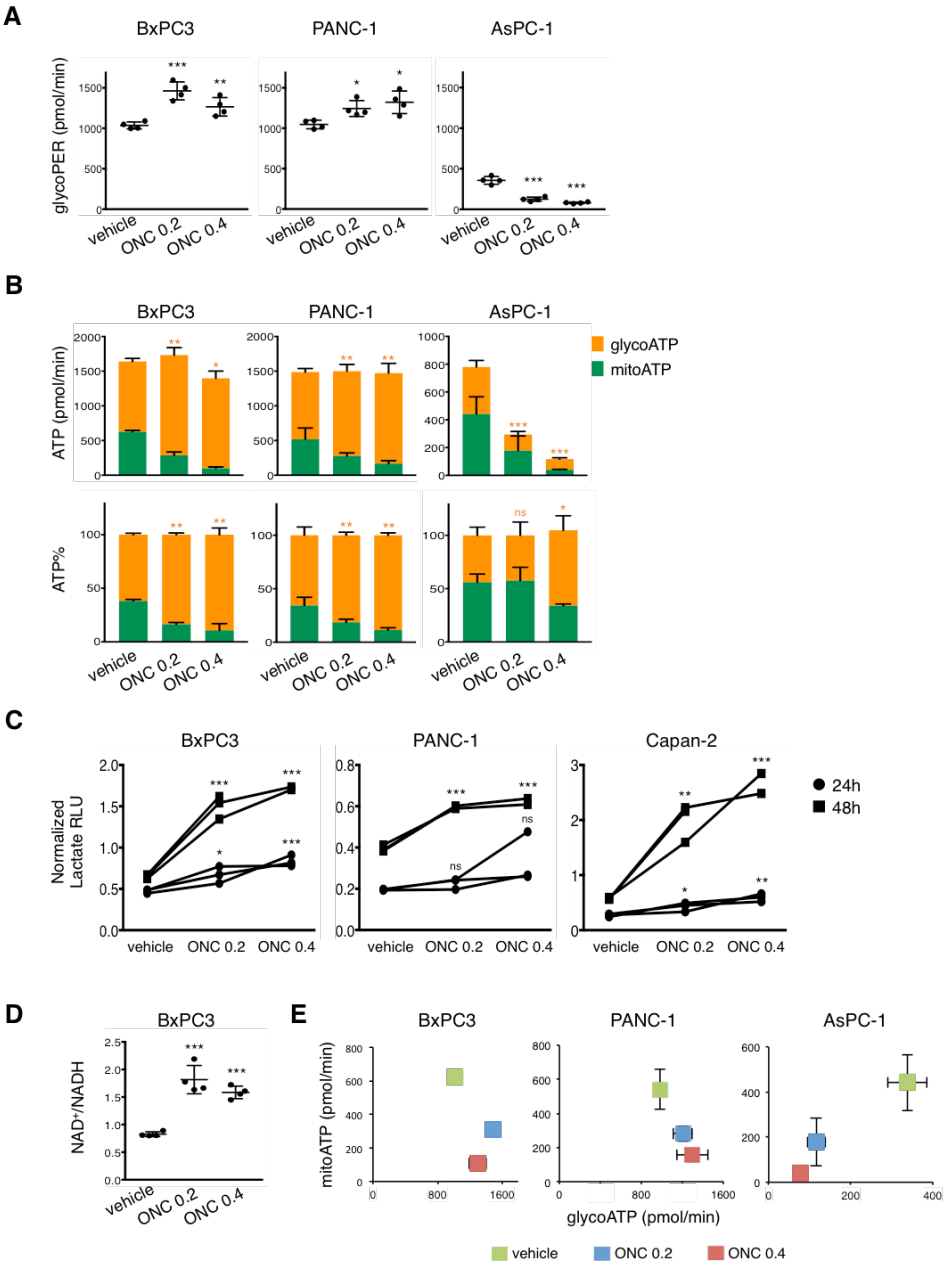

Figure 7. Glycolysis modulation in response to ONC212. (A-B) AsPC-1, BxPC3 and PANC-1 cells were treated for 48 hours with 0.2 or 0.4 µM ONC212 (ONC) prior to performing the ATP Real-Time rate assay. (A) Dot plots showing the glycolytic rate, as measured by glycoPER. **(B)** Bar charts showing the glycolysis-derived (glycoATP) and mitochondria-derived (mitoATP) ATP production rate (*upper panel*). The percentage of ATP generated from each pathway is plotted in the *lower panel*. Means and SD are represented. N = 4 independent experiments. *p<0.05, **p<0.01, ***p<0.001. **(C)** The indicated cell lines were treated with either vehicle or ONC212 at the indicated doses. Lactate RLU was measured after 24 or 48 hours in culture supernatants and normalized to cell viability (expressed in RLU) as measured by CTG assay. N = 3 independent experiments. *p<0.05, **p<0.01, ***p<0.001. **(D)** BxPC3 cells treated or not with ONC212 for 24 hours were permeabilized and the levels of NAD^+ and NADH were individually assessed. NAD^+/NADH ratio is plotted. N = 4 independent experiments. Means and SD are represented. ***p<0.001. **(E)** Energetic maps showing mitoATP production rate and glycoATP production rate of BxPC3, PANC-1 and AsPC-1 cells treated with increasing concentrations of ONC212. Mean and SD of four independent experiments are shown.

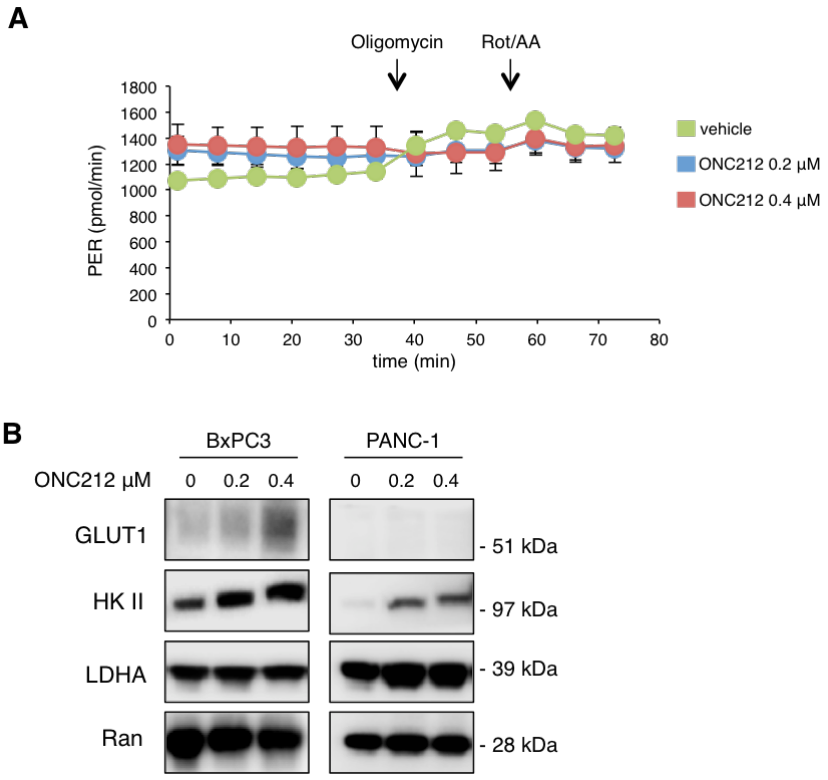

Figure 8. Glycolysis upregulation in BxPC3 and PANC-1 cells. (A) PANC-1 cells were treated for 48 hours with increasing concentrations of ONC212 prior to performing ATP Real-Time rate assay. ONC212-treated cells, characterized by higher glycolytic rate as compared to control, cannot further upregulate PER after oligomycin injection. Mean and SD of three independent experiments are reported. **(B)** Western blot analysis for GLUT1, HK II and LDHA in BxPC3 and PANC-1 cells treated with ONC212 at the indicated concentrations for 48 hours. Blots are representative of two independent experiments.

4.5 Basal mitoATP% may be a new functional biomarker of ONC212 sensitivity

Considering aerobic glycolysis as an oncogenic metabolic pathway potentially counteracting the antineoplastic activity of ONC212, we examined the basal metabolic profile of different cancer cell lines to find possible correlations with ONC212 sensitivity. We discovered that AsPC-1 and HPAF-II cells, displaying the lowest GI50 upon ONC212 treatment as well as ERK1/2 inhibition and PARP cleavage, were predominantly oxidative, as the percentage of mitochondria-derived ATP production (mitoATP% = mitoATP production rate/total ATP production rate * 100) was 56.0% ± 7.7 and 59.5% ± 3.7, respectively. Conversely, the less sensitive BxPC3 and PANC-1 cells were significantly more

glycolytic, with mitoATP% far below 50% (38.2% ± 1.3 and 34.3% ± 7.7, respectively). Therefore, basal mitoATP% could represent a novel, metabolism-based, functional biomarker positively correlating with ONC212 sensitivity (Fig. 9A, B). To further investigate if the cellular metabolic background influenced ONC212 sensitivity, we cultured the less sensitive cell lines (BxPC3, PANC-1 and Capan-2) in glucose-free DMEM containing galactose, which is a well-established method to force cells to use OXPHOS instead of glycolysis to get ATP (37). As shown in Fig. 9C, galactose-cultured cells were more susceptible to ONC212 activity compared to those cultured in standard glucose-containing medium. On the other hand, culturing the most sensitive cells (AsPC-1 and HPAF-II) under hypoxia, which favors a metabolic switch towards glycolysis (38), rendered them more resistant to ONC212 (Fig. 9D). Altogether, these findings suggest that the basal metabolic profile, which is highly dynamic in nature and affected by both cell-intrinsic and environment-based mechanisms, may dictate cell sensitivity to ONC212.

4.6 Glycolysis inhibition converts the cytostatic effect of ONC212 into a pro-apoptotic one

We next evaluated whether ONC212 could trigger cell death in BxPC3 and PANC-1 cells when combined with glycolysis suppression. While cells cultured in glucose were able to sustain ERK1/2 phosphorylation in the presence of ONC212, those grown up in galactose underwent ERK1/2 inhibition after 48-hours of treatment (Fig. 9E). In addition, analysis of PARP cleavage demonstrated that ONC212 could trigger apoptosis when cells were cultured in galactose, while ineffective in apoptosis induction under glucose-containing conditions (Fig. 9E). To further investigate if the simultaneous inhibition of glycolysis could deepen the cytotoxic activity of ONC212, PANC-1 and BxPC3 cells were treated with ONC212 combined with 2-DG, a well-characterized glycolysis inhibitor acting on the first steps of this pathway (39). We found that the combination was highly synergistic in both cell lines, with CI far below 0.5 for various combinatorial doses (Fig. 10A).

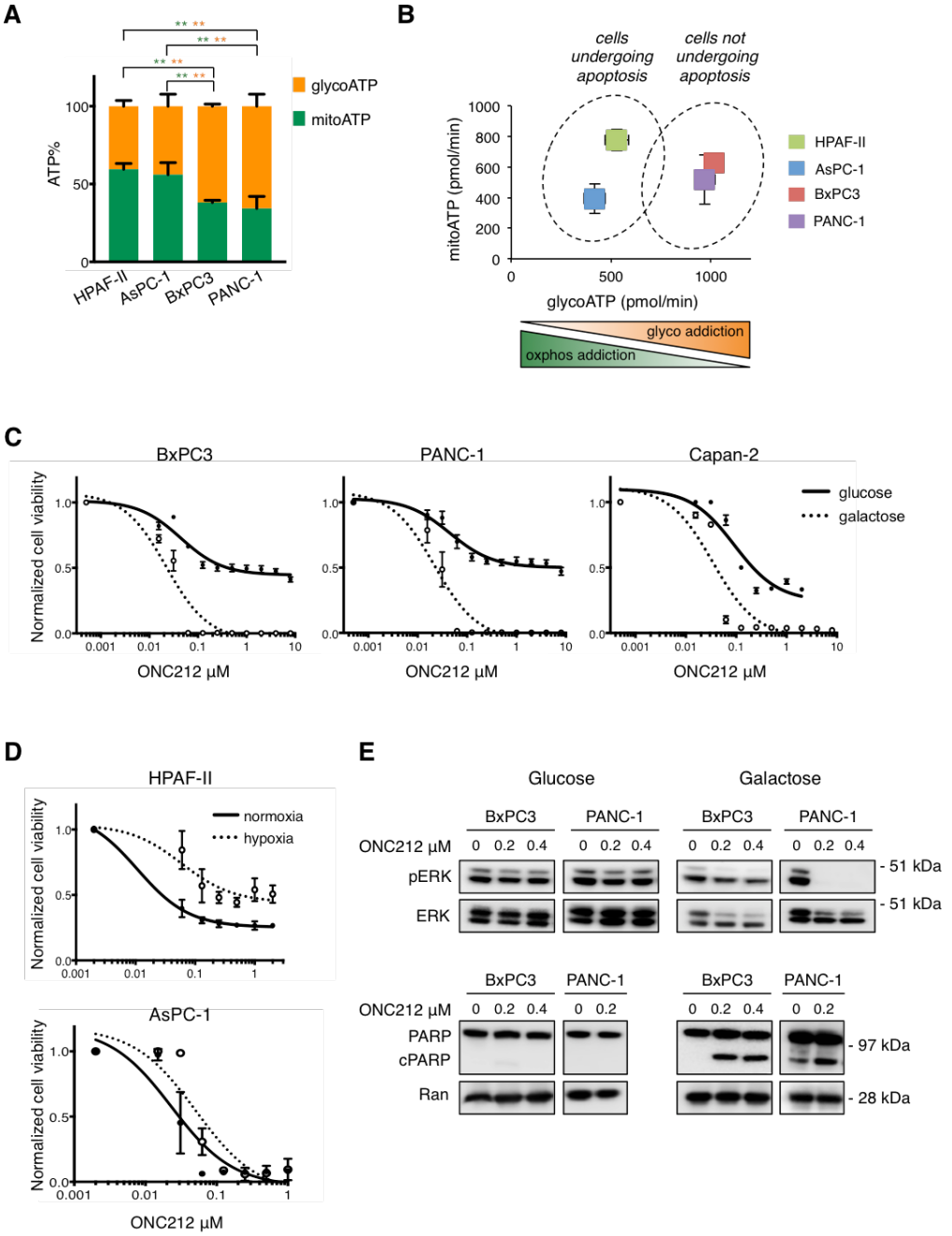

Figure 9. OXPHOS dependence predicts ONC212 sensitivity. (A-B) HPAF-II, AsPC-1, BxPC3 and PANC-1 cells were seeded in a 96-well Seahorse plate at a density of 30000 cells/well. After 48 hours, when cells reached a confluence of about 80 to 90%, the ATP Real-Time rate assay was performed. **(A)** Percentages of mitoATP and glycoATP are shown for each cell line. N = 3 independent experiments. **p<0.01. **(B)** Energetic maps showing the basal metabolic profile of the indicated cell lines. Shown are mean and SD of three independent experiments. **(C)** BxPC3, PANC-1 and Capan-2 cells were cultured in glucose- or galactose-containing medium and treated with increasing concentrations of ONC212 for 72 hours. Cell viability was assessed by CTG assay. Dose-response curves summarizing results from three independent experiments are shown. **(D)** HPAF-II and AsPC-1were treated with increasing concentrations of ONC212 in either normoxia or hypoxia for 72 hours. Cell viability was assessed by CTG assay. Dose-response curves summarizing results from three independent experiments are shown. **(E)** BxPC3 and PANC-1 cells were cultured in glucose- or galactose-containing medium and treated with ONC212 at the indicated concentrations for 48 hours. At the end of culture, western blot analysis for ERK phosphorylation and PARP cleavage was performed.

Importantly, combination treatment, but not ONC212 or 2-DG alone, inhibited ERK1/2 phosphorylation and induced PARP cleavage (Fig. 10B). Therefore, glycolysis sustained the MAPK pathway and promoted apoptotic evasion in the presence of ONC212. In glycolysis-addicted cell lines, shut down of glucose catabolism was needed to turn the cytostatic effect of ONC212 into a pro-apoptotic one (Fig. 10C).

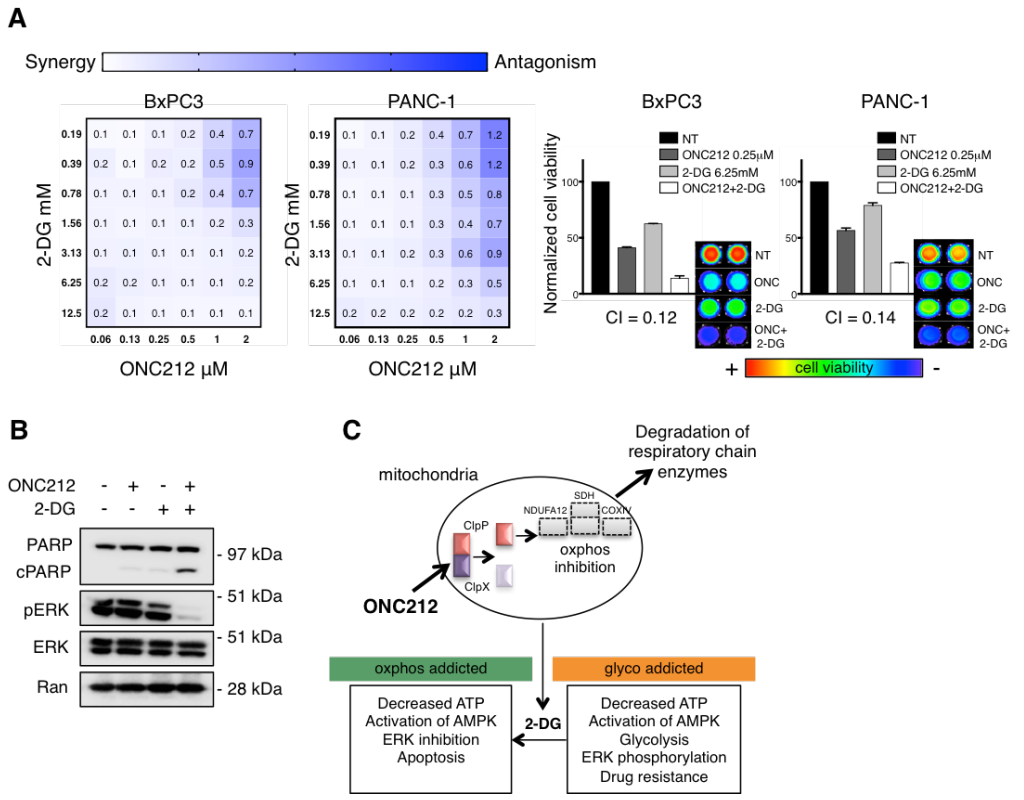

Figura 10. ONC212 synergizes with the glycolysis inhibitor 2-DG *in vitro*. (A) BxPC3 and PANC-1 cells were treated with the combination of ONC212 (0.06-2 µM) and 2-DG (0.19-12.5 mM) for 72 hours. Cell viability was assessed by CTG assay and CI was calculated for each dose combination using Compusyn software. As evidenced by the heat maps (*left panels*), CI is less than 0.5 for most dose combinations, indicating a strong synergism. Graphs (*right panels*) represent a selected synergistic dose of ONC212 and 2-DG, with the corresponding CTG image and CI. **(B)** Western blot analysis of PARP cleavage and ERK phosphorylation in PANC-1 cells treated for 48 hours with vehicle, 0.4 µM ONC212, 25 mM 2-DG or the combination of the two agents. **(C)** Model for conversion of drug-resistant, glycolysis-addicted tumors to apoptotic phenotypes by combining ONC212 with a glycolysis inhibitor, such as 2-DG.

4.7 ONC212 synergizes with 2-DG *in vivo*

To test if the combination of ONC212 and 2-DG could be effective *in vivo*, we generated a xenograft model of pancreatic cancer using the ONC212-resistant BxPC3 cell line. BxPC3 cells were chosen over the PANC1 due to their higher

tumor-forming capacity *in vivo* (30). Once the tumor volume reached at least 100 mm^3, mice were randomly assigned to the treatment with vehicle, ONC212, 2-DG, or the combination. Unlike ONC212 and 2-DG alone, the combination of both agents halted tumor growth in comparison with the control group (P=0.0082 at 30 days after treatment start) (Fig. 11A, B).

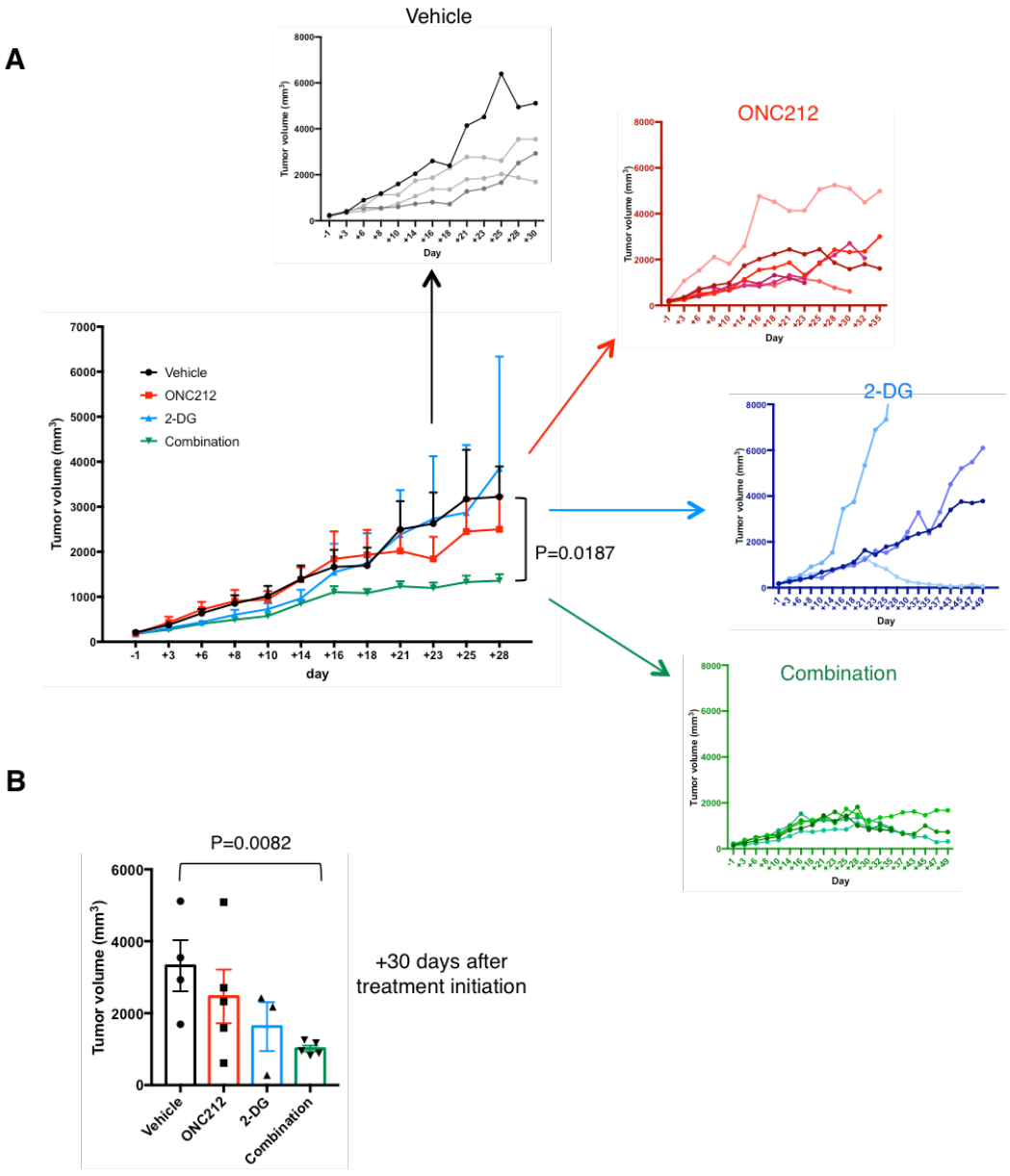

Figure 11. ONC212 synergizes with the glycolysis inhibitor 2-DG *in vivo*. (A) Nude mice subcutaneously xenografted with BxPC3 cells were treated with the indicated agents. Tumor volumes were measured 3 times/week with a digital caliper and graphed until day 28 (main panel, mean ± SEM), as some mice were euthanized later on due to excessive tumor growth. Tumor volume curves of each individual mouse are represented in the smaller panels until the end of the experiment. **(B)** Represented are the tumor volumes measured 30 days after treatment initiation. At this time point, 1 mouse in the ONC212 group and 1 mouse in the 2-DG group had already been sacrificed due to low body weight and excessive tumor growth, respectively. Data are expressed as mean ± SEM.

Moreover, the combination remarkably reduced the variability of tumor growth among mice within the same group, suggesting that simultaneous inhibition of OXPHOS and glycolysis might prevent the metabolic escape from each individual blockade (Fig. 11A).

IHC analysis showed the combination, but not single agents, impaired tumor cell proliferation and increased apoptosis as early as one week after treatment initiation. ERK phosphorylation was also significantly inhibited *in vivo* by ONC212 when combined with 2-DG, whereas the single-agent treatments resulted ineffective (Fig. 12-13).

Blood cell count revealed leukocytopenia in the combination group (Table 2), as a sign of potential bone marrow toxicity selectively involving the white series. Serum chemistry panel showed normal kidney and liver function, with the exception of a mild reduction of total proteins and albumins across all groups, likely due to the tumor itself (Table 3). Also, histological assessment of liver sections did not show any obvious sign of toxicity (Fig. 14A). Monitoring of body weight showed no significant decrease in the combination group, whereas one and two mice in the control and ONC212 groups, respectively, were sacrificed during treatment because of >15% weight loss (Fig. 14B).

Altogether, ONC212 and 2-DG might be an effective and well-tolerated drug combination to target complementary, pro-survival metabolic pathways in pancreatic cancer.

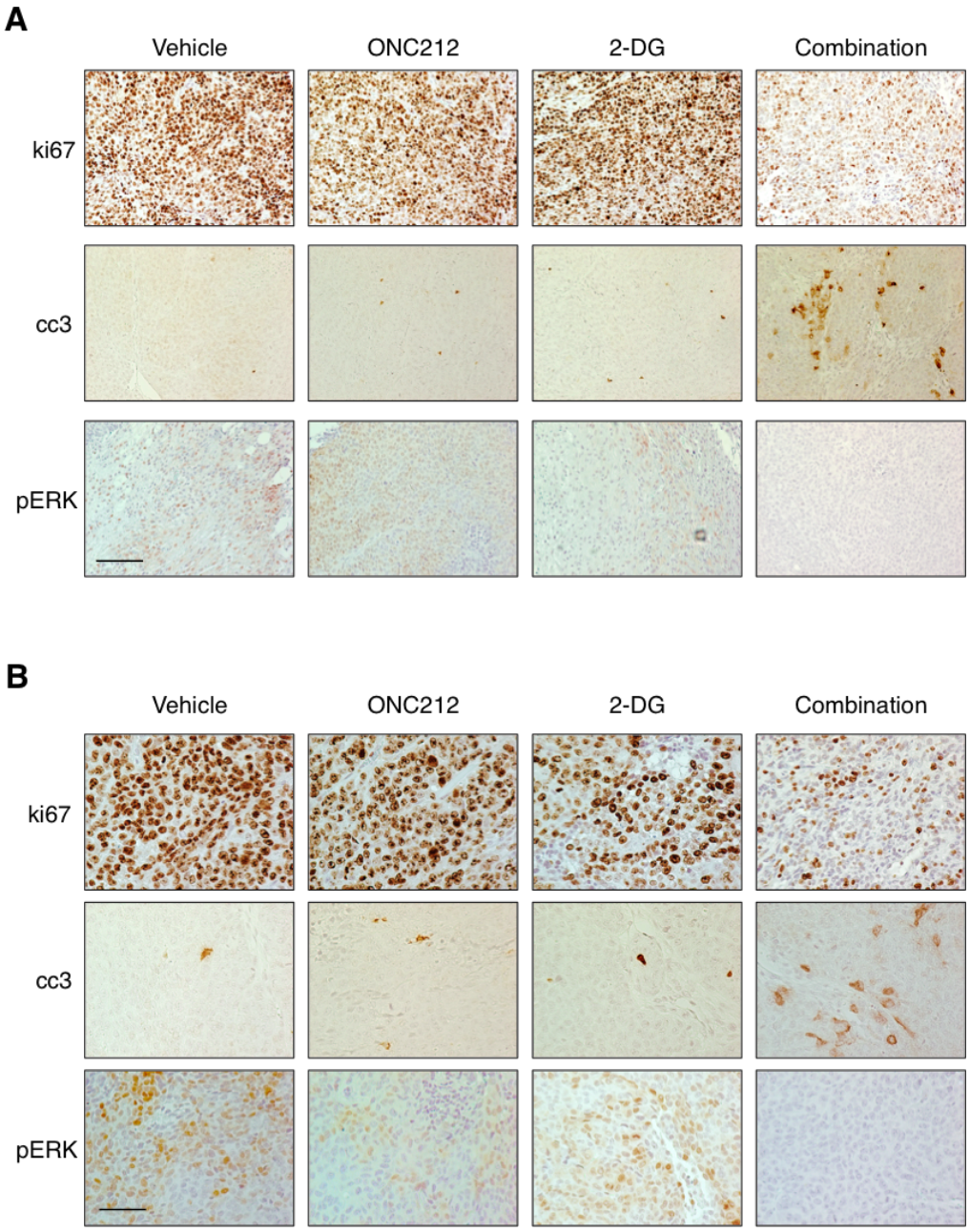

Figure 12. Immunohistochemistry on tumor masses. IHC staining of ki67 (proliferation marker), cleaved caspase 3 (cc3, apoptosis marker) and pERK in BxPC3 xenografts treated with 3 doses of the indicated agents. Images were captured at 20x **(A)** and 40x **(B)** magnification. Scale bar: 100 μm **(A)**, 40 μm **(B)**.

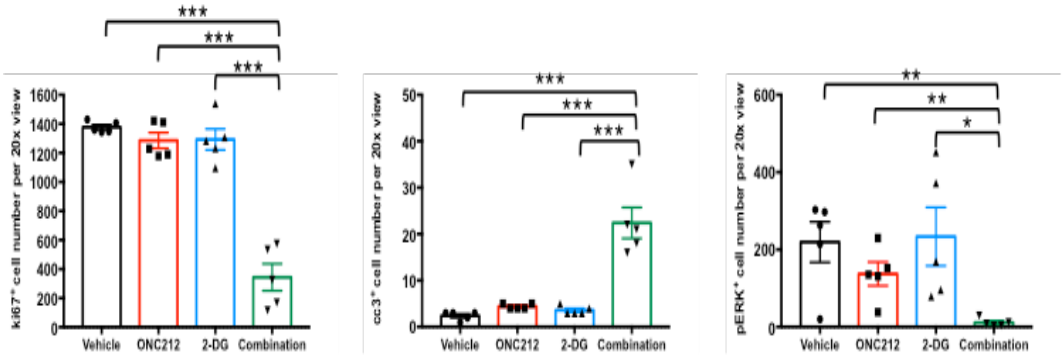

Figure 13. Quantification of immunohistochemistry data. Data are expressed as mean ± SEM. ** p<0.01, ***p<0.001.

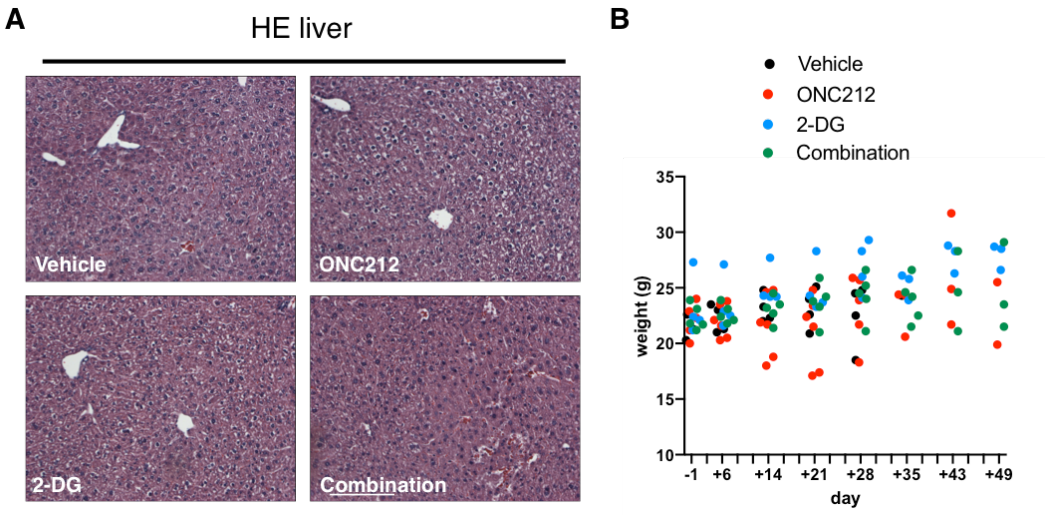

Figure 14. Liver histology and body weight of treated mice. (A) Hematoxylin and eosin (HE) staining of liver sections obtained from mice treated with 3 doses of the indicated agents. 20x magnification. Scale bar: 100 µm. **(B)** Time course analysis of the body weight (g) of mice treated with the indicated agents. Overall, 1 mice in the control group and 2 mice in the ONC212 group were sacrificed due to weight loss >15%.

Table 2. Differential blood cell count of mice treated with ONC212, 2-DG, or the combination of both agents.

	ONC212	2-DG	Combination	Reference range
Hb g/dl	12.8	12.8	12.2	12.8-17.7
PLT x10^3/mmc	811	624	963	691-1400
WBC x10^3/mmc	4.59	2.82	1.33	2.9-15.8
Neu x10^3/mmc	2.81	1.80	0.77	1.02-5.01
Ly x10^3/mmc	1.2	0.79	0.44	1.20-10.87
Mono x10^3/mmc	0.18	0.03	0.03	0.11-0.86
Eo x10^3/mmc	0.23	0.09	0.05	0.01-0.53
Baso x10^3/mmc	0.04	0.02	0.04	0.00-0.21

Table 3. Blood chemistry results of mice treated with ONC212 or the combination of ONC212 and 2-DG.

	ONC212	Combination	Reference range
Creatinine mg/dl	0.2	0.2	0.3-0.5
ALP mmol/L	61	73	57-160
ALT U/L	25	58	35-90
AST U/L	121	148	63-253
Total bilirubin mg/dl	0.2	0.1	0.2-0.6
LDH U/L	607	755	1900-2700
CPK U/L	404	299	620-920
GGT U/L	1	1	2.4-3.2
Total protein g/dl	5.3	4.7	5.3-6.8
Albumin g/dl	3	2.7	3.2-4.3
Calcium mg/dl	9.3	8.4	9.6-11.3
Phosphate mg/dl	8.9	9.5	7-13.2
Cholesterol mg/dl	152	115	87-198
Triglycerides mg/dl	123	231	101-403
Amilase U/L	402	379	5000-8000
Lipase U/L	26	36	700-1100

5. DISCUSSION

With an estimated 5-year survival rate of 9.3%, pancreatic cancer is one of the most lethal human tumors. Standard pharmacological treatment is still based on toxic, yet often unsuccessful, combination chemotherapy with a dearth of effective targeted agents (40). The fluorinated imipridone ONC212 has been recently identified as a novel candidate in pancreatic cancer therapeutics (30). However, the way it counteracts tumor growth, the determinants of its antineoplastic activity and the strategies implemented by cancer cells to survive are not well defined. Our study provides evidence that ONC212 impacts mitochondrial functions and rewires the metabolism of pancreatic cancer cells, acting, de facto, as a novel mitocan (41). In particular, ONC212 a) disrupts ClpXP complex causing profound downregulation of the regulatory subunit ClpX, while leaving unaffected the catalytic subunit ClpP, which is required for its anticancer activity, b) hinders OXPHOS by suppressing critical respiratory chain complex components, c) exerts its cytotoxic effects in a cell- and environment-context dependent manner, with glycolysis emerging as an oncogenic escape metabolic pathway negatively regulating ONC212 sensitivity *in vitro* and *in vivo*.

ClpP, the recently discovered target of imipridones, is an evolutionarily ancient mitochondrial protease often overexpressed in cancer cells (18, 19). Pancreatic cancer cells also broadly express ClpP at the protein level, but its genetic knockdown does not significantly impair cell viability. This contrasts with other cancers such as AML, where ClpP is necessary to maintain cell growth (31). Because ClpP knockdown suppresses mitochondrial metabolism (19), the ability of cancer cells to cope with mitochondrial dysfunction may guide their outcome upon ClpP genetic ablation. The ClpP-binding partner ClpX dramatically decreases upon ONC212 treatment, consistent with previous studies showing that different ClpP-activating compounds displace ClpX and lead to its degradation through yet poorly defined mechanisms (27, 29). Knockdown experiments indicate ClpP is required for ONC212-triggered ClpX suppression. Although this may suggest that aberrantly active ClpP could rapidly degrade its own regulatory

subunit, previously reported cell-free assays have documented that ClpX, unlike casein, is not directly degraded by purified, ONC212-treated ClpP (18). Because we show that cytoplasmic proteasomal and lysosomal degradation plays no role in ClpX downregulation, it is possible that additional proteases residing in the mitochondrial matrix, such as Lon, might be involved in ClpX degradation upon ONC212 exposure. Whether the downregulation of ClpX is critical for ONC212 activity or only represents an epiphenomenon of uncontrolled mitochondrial proteolysis will also need to be clarified in future studies involving ClpX-overexpressing models.

ClpXP dysregulation affects mitochondrial functions. Using immunoblotting and live cell-based metabolic analysis as two complementary approaches, we demonstrated that ONC212 reduces the expression of multiple components of the electron transport chain ultimately leading to OXPHOS collapse. The resulting energetic stress leads to AMPK phosphorylation, a signaling pathway that mammalian cells often use to restore energy imbalance and promote survival (33, 42). Accordingly, AMPK knockdown increases sensitivity to ONC212 at least in PANC-1 cells. This may have interesting translational implications as LKB1, the kinase upstream to AMPK and responsible for its activation, is deleted or mutated in a subset of human cancers showing remarkable sensitivity to energy-stress inducing agents (43). Thus, ONC212 may be particularly powerful against LKB1-disrupted tumors, lacking the ability to cope with energetic stress.

Despite our focus on OXPHOS enzymes, the protease activity of the imipridones' target, whose substrates cover a wide spectrum of proteins involved in several aspects of mitochondrial pathophysiology (18, 31), provides the opportunity to perturb different, mitochondria-centered, homeostatic pathways simultaneously. This may explain why ONC201 and ONC212 have, at least *in vitro*, broad anticancer activity (9) as opposed to most targeted therapies, which usually affect one specific signaling pathway that a particular type of cancer may be addicted to (44). Using functional metabolic approaches, we found that OXPHOS dependency positively correlates with the depth of response to ONC212. The OXPHOS-addicted cell lines AsPC-1 and HPAF-II have the lowest GI50 and undergo

apoptosis upon ONC212 treatment, whereas the glycolysis-addicted BxPC3 and PANC-1 cells undergo growth arrest without apoptosis induction. Essentially, the more oxidative the cancer cells are, the higher their chance of being killed by ONC212. Should our findings be confirmed in larger panels of cell lines and organoids, we may hypothesize to test primary cancer cells or patient-derived organoids for mitoATP production, thus predicting imipridone sensitivity based on tumor-specific metabolic dependence. Future investigations about how ONC212 affects the assembly of respiratory complexes, and how complex-specific mitochondrial respirations are impacted by ONC212 treatment, will better define the metabolic dependencies specifically targeted by this drug. Dihydroorotate dehydrogenase-dependent respiration, which is essential to drive pyrimidine biosynthesis, may be also affected by ONC212 as it shows broad anti-proliferative activity (45). Alternatively to functional metabolic aspects, molecular biomarkers potentially correlating with metabolic signatures could represent a valuable strategy to guide treatment with imipridones in pancreatic cancer. Primary pancreatic tumors and cell lines might express different levels of OXPHOS proteins, indicating different susceptibility to mitochondria-targeting agents. The fact we evaluated only some of the OXPHOS machinery members represents a limitation of our study, which does not permit definitive correlations between the level of OXPHOS proteins and the sensitivity to ONC212. Moreover, in our study the amount of ClpP modulates ONC212 *in vitro* efficacy, suggesting that ClpP levels in primary tumors may predict patients' response to ONC212 treatment.

Our findings in pancreatic cancer cells are in agreement with recent reports highlighting the importance of tumor oxidative metabolism in addition to aerobic glycolysis (21–23), a concept that downsizes Warburg's effect and points to the coexistence of different energy-producing pathways working together and sometimes substituting for each other (24). In our study, glycolysis-addicted cells further increase their glycolytic flux under ONC212. Interestingly, an activator of fungal ClpP termed dioctatin also inhibits oxidative metabolism and enhances *A. flavus* glycolysis and alcohol fermentation, hinting that upregulation of glucose catabolism may be an evolutionarily conserved response to ClpXP perturbation

(46). Such metabolic remodeling sustains ATP production, which is needed, in turn, to keep ERK phosphorylation sufficiently high and avoid cell death. In this regard, our results highlight two basic concepts. First, ERK status under ONC212 is not driven by ONC212 per se, but rather by the cancer cell response to ONC212. Therefore, despite initially described as dual AKT/ERK inhibitors (10), imipridones likely affect these pathways in a cell-context dependent manner. Second, there is bidirectional interplay between the oncogenic Ras-MEK-ERK pathway and glucose metabolism. While KRAS activation drives glycolysis (47), glucose catabolism enhances MAPK signaling, likely supplying ATP and intermediate metabolites fueling the oncogenic cascade (48). Such a compounding cycle can be effectively blocked by the combination of ONC212 and 2-DG, simultaneously inhibiting parallel bioenergetic pathways. Our *in vivo* experiments show this combination is effective in an ONC212-resistant tumor model and devoid of relevant toxicity. This suggests that energy deprivation due to dual inhibition of OXPHOS and glycolysis does have a therapeutic window and proves more lethal in the context of oncogene-driven anabolism as compared to non-transformed cells, which enter a quiescent state allowing them to survive nutrient stress (49). Beside 2-DG, other glycolytic inhibitors may be investigated as potential candidates for combination with ONC212. Among them, LDHA inhibitors could be particularly promising due to their ability to block pyruvate-to-lactate conversion and NAD^+ regeneration, which is essential to fuel the glycolytic flux (50). Furthermore, the combination of ONC212 and clinically-approved MEK inhibitors may be synergistic due to the increased OXPHOS dependency conferred by MAPK inhibition (23).

In addition to cell-intrinsic metabolic background, the surrounding microenvironment, in terms of oxygen and nutrients availability, can influence ONC212 sensitivity. In our study, high levels of glucose and hypoxic environment emerged as extracellular factors negatively impacting ONC212 efficacy. As pancreatic cancer displays intra-tumoral heterogeneity due to different amounts of nutrient and oxygen supply in different neoplastic areas (51), we speculate that cancer cells within the same tumor may respond differently to ONC212 based on their specific localization. Additional experiments investigating ERK status and

apoptotic markers in ONC212-treated cells under normoxia and hypoxia will be required to corroborate our findings.

In conclusion, ONC212 is a novel mitocan acting on the ClpXP complex and causing collapse of mitochondrial bioenergetics. While all pancreatic cancer cells express the target ClpP, only some of them functionally rely on mitochondrial metabolism and are effectively killed by ONC212. Though acting as an escape mechanism in some cell types or specific environmental contexts, glycolysis emerges as a metabolic vulnerability exposed by ONC212 and potentially suitable for strategic drug combinations (Fig. 15).

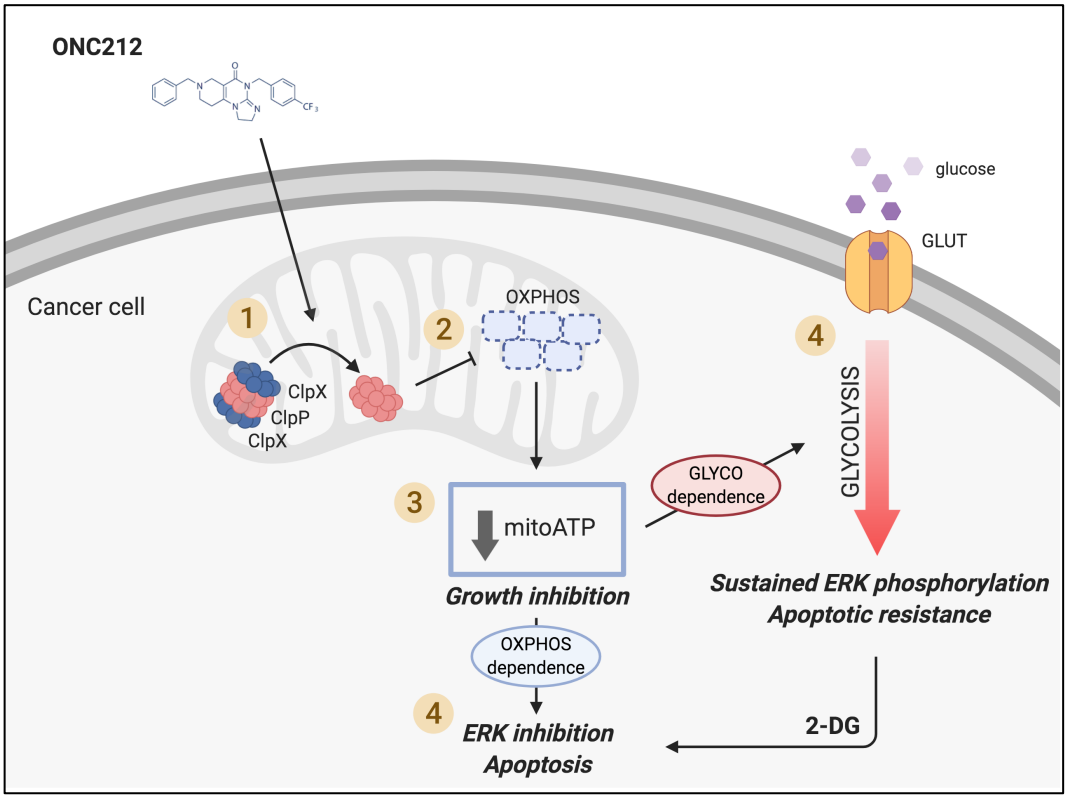

Figure 15. Schematic of ONC212's mode of action in pancreatic cancer. ONC212 interacts with ClpXP complex and leads to rapid degradation of the regulatory subunit ClpX. The catalytic subunit ClpP is hyperactivated by ONC212 and degrades several mitochondrial proteins involved in oxidative phosphorylation (OXPHOS). As a result, mitochondrial ATP production is inhibited and cancer cell growth slows down. In OXPHOS-dependent cells, this is sufficient to suppress ERK phosphorylation and induce apoptosis. By contrast, pancreatic cancer cells relying on aerobic glycolysis further upregulate glucose catabolism in response to ONC212 and ultimately survive the drug. In these cells, the addition of a glycolysis inhibitor such as 2-DG has a synergistic effect and leads to ERK inhibition and apoptosis.

REFERENCES

1. McGuigan A, Kelly P, Turkington RC, Jones C, Coleman HG, and McCain RS. Pancreatic cancer: A review of clinical diagnosis, epidemiology, treatment and outcomes. *World J Gastroenterol* **2018**;24:4846-61.
2. Bailey P, Chang DK, Nones K, Johns AL, Patch AM, Gingras MC, Miller DK, Christ AN, Bruxner TJ, Quinn MC, *et al*. Genomic analyses identify molecular subtypes of pancreatic cancer. *Nature* **2016**;531:47–52.
3. Vaziri-Gohar A, Zarei M, Brody JR and Winter JM (2018) Metabolic Dependencies in Pancreatic Cancer. *Front Oncol* **2018**;8:617.
4. Birsoy K, Possemato R, Lorbeer FK, Bayraktar EC, Thiru P, Yucel B, *et al*. Metabolic determinants of cancer cell sensitivity to glucose limitation and biguanides. *Nature* **2014**;508:108–12.
5. Li X, Li T, Liu Z, Gou S, Wang C. The effect of metformin on survival of patients with pancreatic cancer: a meta-analysis. *Sci Rep* **2017**;7:5825.
6. Nouri K, Feng Y, Schimmer AD. Mitochondrial ClpP serine protease-biological function and emerging target for cancer therapy. *Cell Death Dis,* **2020**;11:841.
7. Gispert, S, Parganlija D, Klinkenberg M, Dröse S, Wittig I, Mittelbronn M, *et al*. Loss of mitochondrial peptidase Clpp leads to infertility, hearing loss plus growth retardation via accumulation of CLPX, mtDNA and inflammatory factors. *Hum Mol Genet* **2013**;22:4871–4887.
8. Jenkinson, EM, Rehman AU, Walsh T, Clayton-Smith J, Lee K, Morell RJ, *et al.* Perrault syndrome is caused by recessive mutations in CLPP, encoding a mitochondrial ATP-dependent chambered protease. *Am J Hum Genet* **2013**;92:605–613.
9. Allen JE, Kline CLB, Prabhu V V, Wagner J, Ishizawa J, Madhukar N, *et al*. Discovery and clinical introduction of first-in-class imipridone. *Oncotarget* **2016**;7:74380-74392
10. Allen JE, Krigsfeld G, Mayes PA, Patel L, Dicker DT, Patel AS, *et al.* Dual Inactivation of Akt and ERK by TIC10 Signals Foxo3a Nuclear Translocation, TRAIL Gene Induction, and Potent Antitumor Effects. *Sci Transl Med* **2013**;5:1–14.
11. Kline CLB, Heuvel APJ Van Den, Allen JE, Prabhu V V, Dicker DT, El-deiry WS. ONC201 kills solid tumor cells by triggering an integrated stress response dependent on ATF4 activation by specific eIF2 a kinases. *Sci Signal* **2016**;9:1–11.
12. Prabhu VV, Morrow S, Rahman Kawakibi A, Zhou L, Ralff M, Ray J, *et al.* ONC201 and imipridones: Anti-cancer compounds with clinical efficacy. *Neoplasia* **2020**;22:725-744.
13. Wagner J, Kline CL, Ralff MD, Lev A, Lulla A, Zhou L, *et al*. Preclinical evaluation of the imipridone family, analogs of clinical stage anti-cancer small molecule ONC201 , reveals potent anti-cancer effects of ONC212. *Cell Cycle* **2017**;16:1790–9.
14. Ishida CT, Zhang Y, Bianchetti E, Shu C, Nguyen TTT, Kleiner G, *et al*. Metabolic Reprogramming by Dual AKT / ERK Inhibition through Imipridones Elicits Unique Vulnerabilities in Glioblastoma. *Clin Cancer Res* **2018**;24:5392–407.

15. Allen JE, Krigsfeld G, Patel L, Mayes PA, Dicker DT, Wu GS. Identification of TRAIL-inducing compounds highlights small molecule ONC201/TIC10 as a unique anti-cancer agent that activates the TRAIL pathway. *Mol Cancer* **2015**;14:99.
16. Kline CLB, Ralff MD, Lulla AR, Wagner JM, Abbosh PH, Dicker DT, *et al*. Role of Dopamine Receptors in the Anticancer Activity of ONC201. *Neoplasia* **2018**;20:80-91.
17. Nii T, Prabhu V V, Ruvolo V, Madhukar N, Zhao R, Mu H, *et al.* Imipridone ONC212 activates orphan G protein-coupled receptor GPR132 and integrated stress response in acute myeloid leukemia. *Leukemia* **2019**;33:2805-2816.
18. Ishizawa J, Zarabi SF, Davis RE, Halgas O, Nii T, Jitkova Y, *et al.* Mitochondrial ClpP-Mediated Proteolysis Induces Selective Cancer Cell Lethality Article Mitochondrial ClpP-Mediated Proteolysis Induces Selective Cancer Cell Lethality. *Cancer Cell* **2019**;35:721–37.
19. Seo JH, Rivadeneira DB, Caino MC, Chae YC, Speicher W, Tang H, *et al*. The Mitochondrial Unfoldase-Peptidase Complex ClpXP Controls Bioenergetics Stress and Metastasis. *PLoS Biol* **2016**;14:e1002507.
20. Pruss M, Dwucet A, Tanriover M, Hlavac M, Kast RE, Debatin K, *et al*. Dual metabolic reprogramming by ONC201 / TIC10 and 2-Deoxyglucose induces energy depletion and synergistic anti-cancer activity in glioblastoma. *Br J Cancer* **2020**;122:1146-1157.
21. Kashatus JA, Nascimento A, Myers LJ, Sher A, Byrne FL, Hoehn KL, *et al.* Erk2 phosphorylation of Drp1 promotes mitochondrial fission and MAPK-driven tumor growth. Mol Cell **2015**;57:537-51.
22. Yu M, Nguyen ND, Huang Y, Lin D, Fujimoto TN, Molkentine JM, *et al.* Mitochondrial fusion exploits a therapeutic vulnerability of pancreatic cancer. *JCI Insight* **2019**;5.pii:126915
23. Viale A, Pettazzoni P, Lyssiotis CA, Ying H, Sánchez N, Marchesini M, *et al.* Oncogene ablation-resistant pancreatic cancer cells depend on mitochondrial function. *Nature* **2014**;514:628-32.
24. Deberardinis RJ, Chandel NS. Fundamentals of cancer metabolism. *Sci Adv* **2016**;2:e1600200.
25. Bankhead P, Maurice B. Fernández LJA, Dombrowski Y, McArt DG, Dunne PD, *et al.* QuPath: Open source software for digital pathology image analysis. *Sci Rep* **2017**;7:16878.
26. Pingping Hou, Avnish Kapoor, Qiang Zhang, Jiexi Li, Chang-Jiun Wu, Jun Li, *et al.* Tumor Microenvironment Remodeling Enables Bypass of Oncogenic KRAS Dependency in Pancreatic Cancer. *Cancer Discov* **2020**;10:1058-1077.
27. Jacques S, van der Sloot AM, C Huard C, Coulombe-Huntington J, Tsao S, Tollis S, *et al.* Imipridone Anticancer Compounds Ectopically Activate the ClpP Protease and Represent a New Scaffold for Antibiotic Development. *Genetics* **2020**;214:1103-1120.
28. Graves PR, Aponte-collazo LJ, Fennell EMJ, Graves AC, Hale AE, Dicheva N, *et al.* Mitochondrial Protease ClpP is a Target for the Anticancer Compounds ONC201 and Related Analogues. *ACS Chem Biol* **2019**;14:1020-1029.

29. Wong KS, Mabanglo MF, Seraphim TV, Mollica A, Mao YQ, Rizzolo K, *et al*. Acyldepsipeptide Analogs Dysregulate Human Mitochondrial ClpP Protease Activity and Cause Apoptotic Cell Death. *Cell Chem Biol* **2018**;25:1017-1030.
30. Lev A, Lulla AR, Wagner J, Ralff MD, Kiehl JB, Zhou Y, *et al*. Anti-pancreatic cancer activity of ONC212 involves the unfolded protein response (UPR) and is reduced by IGF1-R and GRP78/BIP. *Oncotarget* **2017**;8:81776–93.
31. Cole A, Wang Z, Coyaud E, Voisin V, Gronda M, Jitkova Y, *et al*. Inhibition of the Mitochondrial Protease ClpP as a Therapeutic Strategy for Human Acute Myeloid Leukemia. *Cancer Cell* **2015;**27:864-76.
32. https://www.proteinatlas.org/ENSG00000125656-CLPP/pathology
33. Hardie DG, Ross FA, Hawley SA. AMPK: a nutrient and energy sensor that maintains energy homeostasis. *Nat Rev Mol Cell Biol* **2012**;13:251-62.
34. Gysin S, Lee S, Dean NM, Mcmahon M. Pharmacologic inhibition of RAF-->MEK-->ERK signaling elicits pancreatic cancer cell cycle arrest through induced expression of p27Kip1. *Cancer Res* **2005**;65:4870-4880.
35. Hay N. Reprogramming glucose metabolism in cancer : can it be exploited for cancer therapy? *Nat Rev Cancer* **2016**;16:635-49.
36. Apicella M, Giannoni E, Fiore S, Ferrari KJ, Fernández-Pérez D, Isella C, *et al.* Increased Lactate Secretion by Cancer Cells Sustains Non-cell-autonomous Adaptive Resistance to MET and EGFR Targeted Therapies. *Cell Metab* **2018**;28:848-865.
37. Aguer C, Gambarotta D, Mailloux RJ, Moffat C, Dent R, McPherson R, *et al.* Galactose Enhances Oxidative Metabolism and Reveals Mitochondrial Dysfunction in Human Primary Muscle Cells. *PLoS One* **2011**;6:e28536.
38. Nagao A, Kobayashi M, Koyasu S, Chow CCT, Harada H. HIF-1-Dependent Reprogramming of Glucose Metabolic Pathway of Cancer Cells and Its Therapeutic Significance. *Int J Mol Sci* 2019;20.pii:E238.
39. Rashmi R, Huang X, Floberg JM, Elhammali AE, Mccormick ML, Patti GJ, *et al.* Radioresistant Cervical Cancers Are Sensitive to Inhibition of Glycolysis and Redox Metabolism. *Cancer Res* **2018**;78:1392-1403.
40. Gromisch C, Qadan M, Albuquerque Machado M, Liu K, Colson Y, Grinstaff MW. Pancreatic Adenocarcinoma: Unconventional Approaches for an Unconventional Disease. *Cancer Res* **2020**;pii:canres.2731.2019.
41. Neuzil J, Dong L, Rohlena J, Truksa J, Ralph SJ. Classification of mitocans, anti-cancer drugs acting on mitochondria. *Mitochondrion* **2013**;13:199–208
42. Greer YE, Porat-Shliom N, Nagashima K, Stuelten C, Crooks D, Koparde VN, *et al.* ONC201 Kills Breast Cancer Cells in vitro by Targeting Mitochondria. *Oncotarget* **2018**;9:18454-18479.
43. Momcilovic M, Shackelford DB. Targeting LKB1 in cancer – exposing and exploiting vulnerabilities. *Br J Cancer* **2015**;113:574-84.
44. Gross S, Lengauer C, Hoeflich KP, Lengauer C, Hoeflich KP. Targeting cancer with kinase inhibitors. *J Clin Invest* **2015**;125:1780–9.
45. Bajzikova M, Kovarova J, Coelho AR, Boukalova S, Oh S, Rohlenova K, *et al.* Reactivation of Dihydroorotate Dehydrogenase-Driven Pyrimidine Biosynthesis Restores Tumor Growth of Respiration-Deficient Cancer

Cells. *Cell Metab* **2019**;29:399-416.
46. Furukawa T, Katayama H, Oikawa A, Negishi L, Ichikawa T, Suzuki M, *et al*. Dioctatin Activates ClpP to Degrade Mitochondrial Components and Inhibits Aflatoxin Production. *Cell Chem Biol* **2020**; doi: 10.1016/j.chembiol.2020.08.006.
47. Amendola CR, Mahaffey JP, Parker SJ, Ahearn IM, Chen W, Zhou M, *et al.* KRAS4A directly regulates hexokinase 1. *Nature* **2019**;576:482-486.
48. Peeters K, Leemputte F Van, Fischer B, Bonini BM, Quezada H, Tsytlonok M, *et al.* Fructose-1,6-bisphosphate couples glycolytic flux to activation of Ras. *Nat Commun.* **2017**;8:922.
49. Kim SM, Roy SG, Chen B, Nguyen TM, McMonigle RJ, McCracken AN, *et al.* Targeting cancer metabolism by simultaneously disrupting parallel nutrient access pathways. *J Clin Invest* **2016**;126:4088-4102.
50. Boudreau A, Purkey HE, Hitz A, Robarge K, Peterson D, Labadie S, *et al*. Metabolic plasticity underpins innate and acquired resistance to LDHA inhibition. *Nat Chem Biol.* **2016**;12:779-786.
51. Maley CC, Aktipis A, Graham TA, Sottoriva A, Boddy AM, Janiszewska M, *et al.* Classifying the evolutionary and ecological features of neoplasms. *Nat Rev Cancer* **2017**;17:605-619.